Article

Immunity

Potently neutralizing and protective anti-human metapneumovirus antibodies target diverse sites on the fusion glycoprotein

Graphical abstract

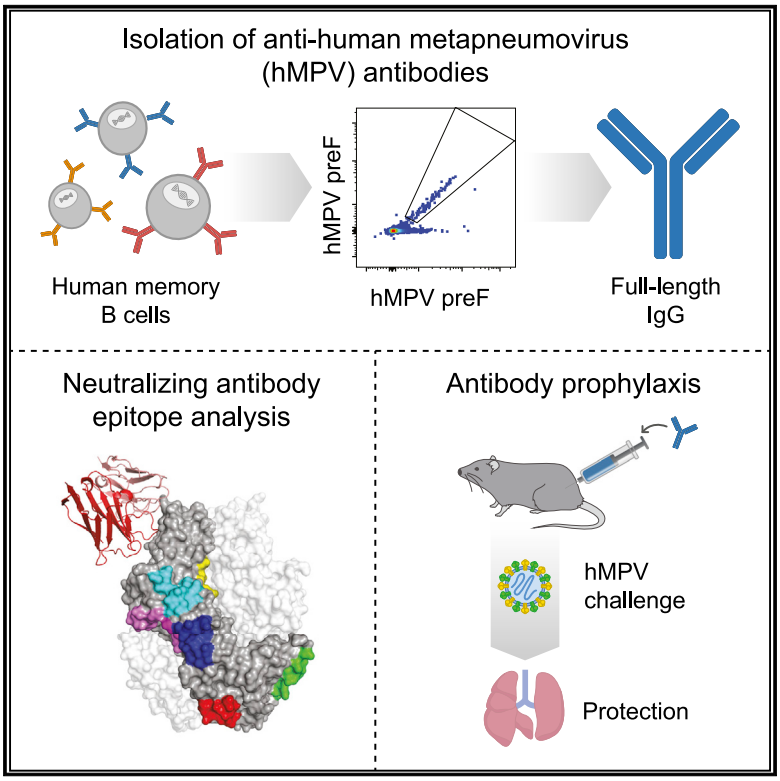

Authors

C. Garrett Rappazzo, Ching-Lin Hsieh, Scott A. Rush, ..., Vicente Más, Jason S. McLellan, Laura M. Walker

Correspondence

jmclellan@austin.utexas.edu (J.S.M.), lwalker@adagiotx.com (L.M.W.)

In brief

Rappazzo et al. isolate and structurally characterize monoclonal antibodies from human metapneumovirus convalescent donors that display broad and potent neutralization and recognize distinct sites on the fusion glycoprotein. Multiple antibodies demonstrate robust prophylactic efficacy in a small animal model. The results provide a framework for the development of hMPV vaccines and therapeutics.

Highlights

- 375 antibodies from hMPV preF-reactive MBCs characterized as full-length IgGs
- Neutralizing antibodies predominately target epitopes conserved on postF conformation
- Structural analysis of a rare preF-specific neutralizer defines a F trimer apex epitope
- 3 potent neutralizers targeting non-overlapping epitopes protect from hMPV challenge

Rappazzo et al., 2022, Immunity *55*, 1710–1724
September 13, 2022
https://doi.org/10.1016/j.immuni.2022.07.003

CellPress

CellPress
OPEN ACCESS

Immunity

Article

Potently neutralizing and protective anti-human metapneumovirus antibodies target diverse sites on the fusion glycoprotein

C. Garrett Rappazzo,[1] Ching-Lin Hsieh,[2] Scott A. Rush,[2] Emma S. Esterman,[1] Teresa Delgado,[3] James C. Geoghegan,[1] Anna Z. Wec,[1] Mrunal Sakharkar,[1] Vicente Más,[3] Jason S. McLellan,[2,*] and Laura M. Walker[4,5,*]

[1]Adimab, LLC, Lebanon, NH 03766, USA
[2]Department of Molecular Biosciences, The University of Texas at Austin, Austin, TX 78712, USA
[3]Centro Nacional de Microbiología, Instituto de Salud Carlos III, 28220 Madrid, Spain
[4]Adagio Therapeutics, Inc., Waltham, MA 02451, USA
[5]Lead contact
*Correspondence: jmclellan@austin.utexas.edu (J.S.M.), lwalker@adagiotx.com (L.M.W.)
https://doi.org/10.1016/j.immuni.2022.07.003

SUMMARY

Human metapneumovirus (hMPV) is a leading cause of acute lower respiratory tract infections in high-risk populations, yet there are no vaccines or anti-viral therapies approved for the prevention or treatment of hMPV-associated disease. Here, we used a high-throughput single-cell technology to interrogate memory B cell responses to the hMPV fusion (F) glycoprotein in young adult and elderly donors. Across all donors, the neutralizing antibody response was primarily directed to epitopes expressed on both pre- and post-fusion F conformations. However, we identified rare, highly potent broadly neutralizing antibodies that recognize pre-fusion-specific epitopes and structurally characterized an antibody that targets a site of vulnerability at the pre-fusion F trimer apex. Additionally, monotherapy with neutralizing antibodies targeting three distinct antigenic sites provided robust protection against lower respiratory tract infection in a small animal model. This study provides promising monoclonal antibody candidates for passive immunoprophylaxis and informs the rational design of hMPV vaccine immunogens.

INTRODUCTION

Human metapneumovirus (hMPV), a pneumovirus discovered in 2001, is a leading cause of hospitalizations due to acute lower respiratory tract infections (Afonso et al., 2016; Panda et al., 2014; van den Hoogen et al., 2001). Primary exposure to hMPV typically occurs before age 5 (Edwards et al., 2013; van den Hoogen et al., 2001) and is responsible for 6%–40% of respiratory infections among hospitalized and outpatient children (Shafagati and Williams, 2018), second only to respiratory syncytial virus (RSV) (Anderson et al., 2012; Foulongne et al., 2006). Furthermore, reinfections occur throughout life and can cause severe illness in adults, particularly in elderly and immunocompromised individuals, with hospitalization rates comparable to RSV and influenza (Falsey et al., 2003; Haas et al., 2013; Shafagati and Williams, 2018; Widmer et al., 2012). However, there are currently no vaccines or specific anti-viral therapies approved for the prevention or treatment hMPV-associated disease. This contrasts with its close evolutionary relative, RSV, for which the monoclonal antibody (mAb) palivizumab has been approved for passive prophylaxis in high-risk infants since 1998 (The IMpact-RSV Study Group, 1998) and for which additional mAbs and vaccines have shown promise in clinical trials (Alipprantis et al., 2021; Hammitt et al., 2022; Ruckwardt et al., 2021; Sadoff et al., 2021). Nevertheless, the common sequence and structural elements shared between RSV and hMPV, as well as their similar clinical courses of disease, suggest that analogous prophylactic interventions may be effective in the prevention of hMPV infections.

Similar to RSV, hMPV encodes three surface glycoproteins: the attachment (G), small hydrophobic (SH), and the fusion (F) glycoproteins. The hMPV F glycoprotein is required for infection and is the only known target of neutralizing antibodies (Huang et al., 2019; Skiadopoulos et al., 2006). HMPV F is synthesized as an inactive precursor, F_0, that is cleaved by trypsin-like proteases to generate two subunits, F_2 and F_1, that remain covalently linked by disulfide bonds (Shirogane et al., 2008). Mature hMPV F is a trimer of disulfide-linked heterodimers that adopts a metastable pre-fusion (preF) conformation, and neutralizing antibodies inhibit its transition to an energetically favored post-fusion (postF) conformation, thereby preventing viral fusion with host cells (Battles et al., 2017; Más et al., 2016; White et al., 2008). The F protein is also highly conserved across the two genetic lineages of hMPV (subtypes A and B) and their sub-lineages (subgroups A1, A2, B1, and B2) (Nao et al., 2020; van den Hoogen et al., 2004a; Yang et al., 2009).

Furthermore, hMPV and RSV F are structurally similar and share approximately 33% sequence identity (van den Hoogen et al., 2002), providing opportunities for antibody cross-neutralization (Corti et al., 2013; Gilman et al., 2016; Mas et al., 2018; Más et al., 2016; Mousa et al., 2018; Schuster et al., 2015; Wen et al., 2017).

Despite their high degree of sequence and structural similarity, previous serum-mapping studies have revealed key differences in the antibody response to hMPV and RSV F. The serum-neutralizing antibody response to RSV is dominated by antibodies that bind exclusively to preF (Magro et al., 2012; Ngwuta et al., 2015), whereas anti-hMPV-serum-neutralizing antibodies appear to recognize both preF and postF (Battles et al., 2017; Huang et al., 2021). In addition, while the most potently neutralizing RSV F-specific antibodies target antigenic sites located at the apex of the preF trimer (sites Ø and V) (Gilman et al., 2016), these sites are shielded by N-linked glycans on hMPV F (Battles et al., 2017). Consequently, no hMPV F-specific human mAbs targeting analogous antigenic sites at the apex of the preF trimer have been identified to date (Huang et al., 2019). Lastly, although RSV preF elicits substantially higher serum-neutralizing antibody titers than postF in animal models (McLellan et al., 2013a), immunization with similarly stabilized hMPV preF antigens does not elicit higher hMPV serum-neutralizing antibody titers than vaccination with hMPV postF (Battles et al., 2017; Pilaev et al., 2020). Although these studies have provided insights into hMPV-F-specific serum antibody responses, the frequencies, potencies, fine specificities, and cross-reactivities of human memory B cell (MBC)-derived antibodies induced by natural hMPV infection remain undefined.

Here, we mined the MBC repertoires of 16 hMPV convalescent donors to isolate and characterize antibodies specific for the hMPV F protein. We report that the MBC response is primarily directed to 7 distinct antigenic sites on the F protein, several of which are associated with potent antibody neutralization. Structural studies of a rare, highly potent broadly neutralizing preF-specific antibody illuminated an immunoquiescent site of vulnerability at the apex of the pre-fusion F trimer, providing a target for rational hMPV vaccine design. This antibody, as well as two additional potently neutralizing antibodies directed to non-overlapping antigenic sites on hMPV F, provided robust prophylactic protection against lower respiratory tract infection in a small animal model. Together, our findings provide fundamental insights into the human B cell response to hMPV F and may inform the development of mAb-based therapeutics and hMPV vaccines tailored to elicit protective antibody responses.

RESULTS

Healthy donors exhibit serum and MBC responses to hMPV F

To study the human B cell response to hMPV F in naturally infected donors, we collected serum and peripheral blood mononuclear cell (PBMC) samples from 8 elderly (aged > 65 years) and 8 young adult (aged 21–27 years) donors (Table S1). All donor sera displayed IgG-binding reactivity with hMPV preF from both subgroups A1 and B2 and postF from subgroup A1 (Figure 1A). In addition, all donor sera neutralized GFP-recombinant hMPV viruses derived from isolates A1 NL/1/00 and B1 NL/1/99 (de Graaf et al., 2007; Figure 1B). There were no significant differences in serum anti-hMPV F-binding or -neutralizing activity between the two age cohorts, although one elderly donor with a clinical history of severe hMPV-associated disease (IML2992) displayed notably elevated serum IgG binding and neutralization relative to the other donors (Table S1; Figures 1A and 1B).

Although serum-neutralizing antibodies to hMPV often recognize both pre- and post-fusion conformations of F, binding to preF is required for neutralization (Battles et al., 2017). Therefore, we focused our B cell isolation efforts on MBCs reactive with the pre-fusion conformation of F. We stained PMBC samples from each donor with fluorescently labeled tetramers of hMPV preF and quantified antigen-specific B cells by flow cytometry (Figures 1C and S1A). As expected, we detected hMPV preF-specific MBCs in all donors, with frequencies ranging from 0.07% to 3.69% of class-switched (swIg$^+$) B cells (Figures 1D and S1B). Given the sequence and structural similarities between RSV and hMPV F, we also determined the frequency of RSV/hMPV cross-reactive B cells using dual-antigen labeling (Figures 1C and S1A). In all donors, RSV preF cross-reactive cells comprised a minority of the hMPV preF-reactive swIg$^+$ B cell population, with a median of 3.08% and range of 0%–12.2% (Figures 1E and S1B). Notably, the proportion of cross-reactive B cells trended higher in the elderly cohort but did reach statistical significance ($p = 0.11$).

HMPV F-specific MBC repertoires possess diverse sequence features

To further dissect the MBC response to hMPV preF, we single-cell sorted hMPV preF-reactive swIg$^+$ B cells from 3 elderly and 3 young adult donors with the highest frequencies of hMPV preF-reactive MBCs for antibody isolation (Figures 2A, S1B, and S2A). In total, we cloned and expressed 435 natively paired mAbs as full-length IgG1 proteins in an engineered strain of *S. cerevisiae* (Sakharkar et al., 2021), of which 375 were confirmed to bind to hMPV F by biolayer interferometry (BLI) (Table S2). Index sorting analysis revealed that most (64%–96%) of the binding antibodies originated from IgG$^+$ B cells, of which the majority (75%–97%) expressed the canonical MBC marker CD27 (Figure S2B).

Sequence analysis of the isolated mAbs revealed that the hMPV preF-reactive MBC repertoires were highly diverse across all donors. The mAbs utilized a broad diversity of heavy-chain variable region (VH) germline genes, with only VH1-18 consistently over-represented relative to previously published baseline human B cell repertoires (Vander Heiden et al., 2017; Table S2; Figure 2B). The mAbs also belonged to diverse clonal lineages, with clonal expansions representing only 4%–26% of each donor repertoire (Figure 2C). The degree of antibody somatic hypermutation (SHM) was similar across individual donors and between the two age cohorts, with median SHM loads ranging from 17 to 22 nucleotide substitutions in VH (Table S2; Figure 2D). These SHM loads are comparable to those observed in antibodies induced by secondary viral infections, such as influenza and RSV (Gilman et al., 2016; Wrammert et al., 2008), and is consistent the recurrent nature of hMPV infections (Shafagati and Williams, 2018). We conclude that hMPV F-specific MBC

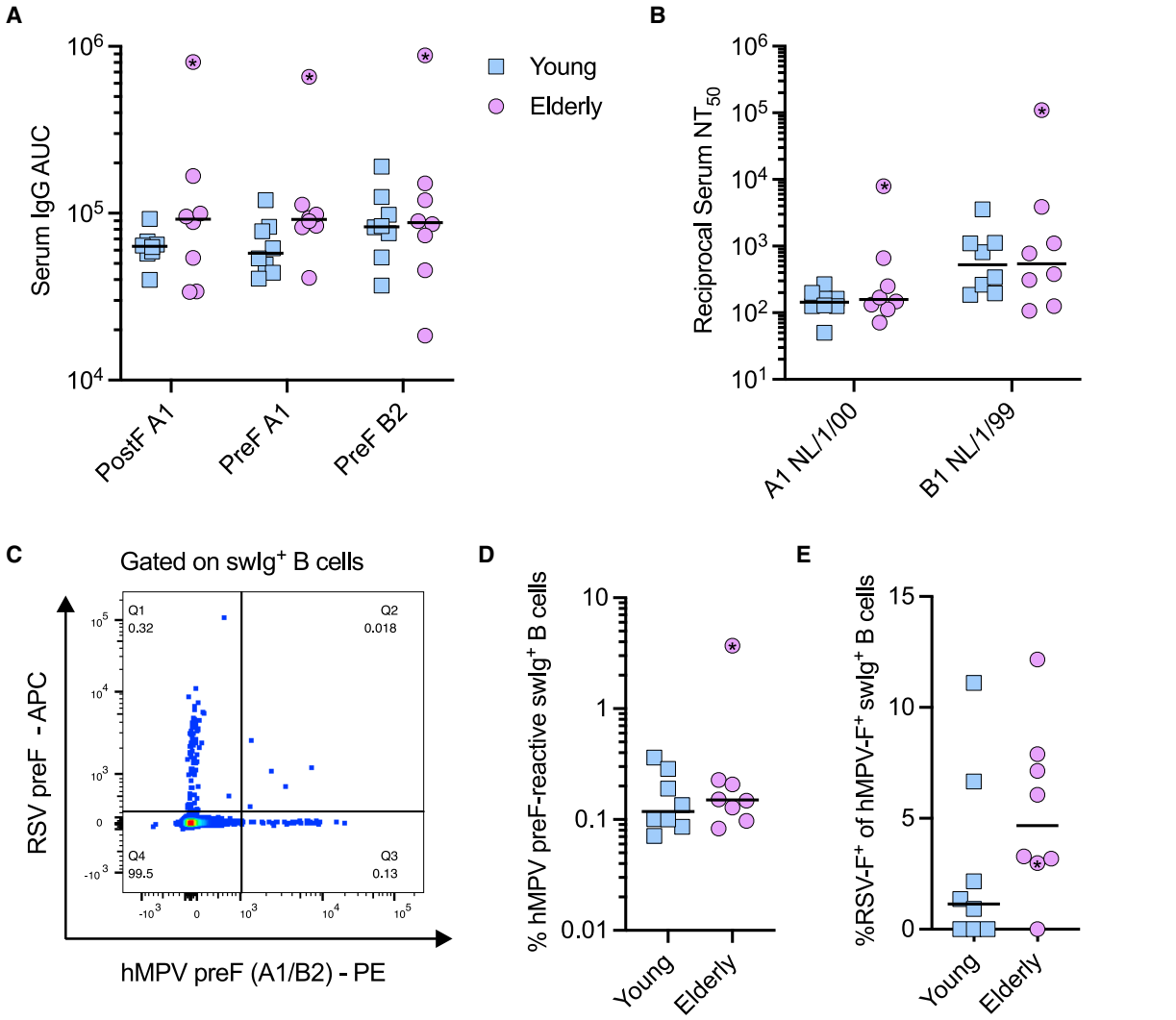

Figure 1. Healthy donors exhibit serum and MBC responses to hMPV and RSV F

(A) Serum IgG binding to the indicated pre-fusion (preF) or post-fusion (postF) hMPV F antigens, as assessed by ELISA.

(B) Serum half-maximal neutralizing titers (NT_{50}) for the indicated GFP-expressing recombinant hMPV isolates.

(C) Representative fluorescence-activated cell sorting (FACS) plot for the identification and enumeration of hMPV and/or RSV preF-reactive $swIg^+$ B cells.

(D) Frequencies of hMPV preF-reactive cells among $swIg^+$ $CD19^+$ B cells, as determined by flow cytometry.

(E) Frequencies of RSV preF cross-reactive cells among hMPV preF-specific $swIg^+$ B cells. Black bars indicate medians. Samples from 16 healthy donors were assessed across two independent experiments. Asterisks denote a donor (IML2992) with a clinical history of severe hMPV-associated disease. Statistical comparisons were performed by two-sided Mann-Whitney U tests. AUC, area under the curve; $swIg^+$, class switched.

See also Table S1 and Figure S1.

repertoires are genetically diverse and possess sequence features suggestive of repeated antigenic stimulation in both young adult and elderly donors.

Most hMPV preF-specific antibodies are weakly neutralizing

We next evaluated the binding affinities of the isolated mAbs to recombinant hMPV preF and postF by BLI. The antigen-binding fragments (Fabs) of antibodies isolated from each donor displayed similar binding affinities for hMPV preF A1, with geometric mean K_Ds of 0.59–2.42 and 0.60–1.23 nM in young adult and elderly donors, respectively (Figure S3A). Overall, 62% (236/375) of mAbs bound exclusively to preF, representing the majority (54%–77%) of each donor repertoire (Table S2; Figures 3A and 3B). All but one of the remaining mAbs bound to both preF and postF, although a proportion of mAbs displayed preferential binding to one conformation of F (Figures 3A and 3B).

Consistent with the high degree of F glycoprotein amino acid sequence identity between hMPV subgroups A1 and B2 (>94%) (Yang et al., 2009), 83%–98% of mAbs isolated from each donor displayed reactivity to both hMPV preF A1 and B2 (Table S2; Figure 3C). In contrast, only 0%–3.5% of mAbs from each donor repertoire displayed cross-reactivity with RSV preF

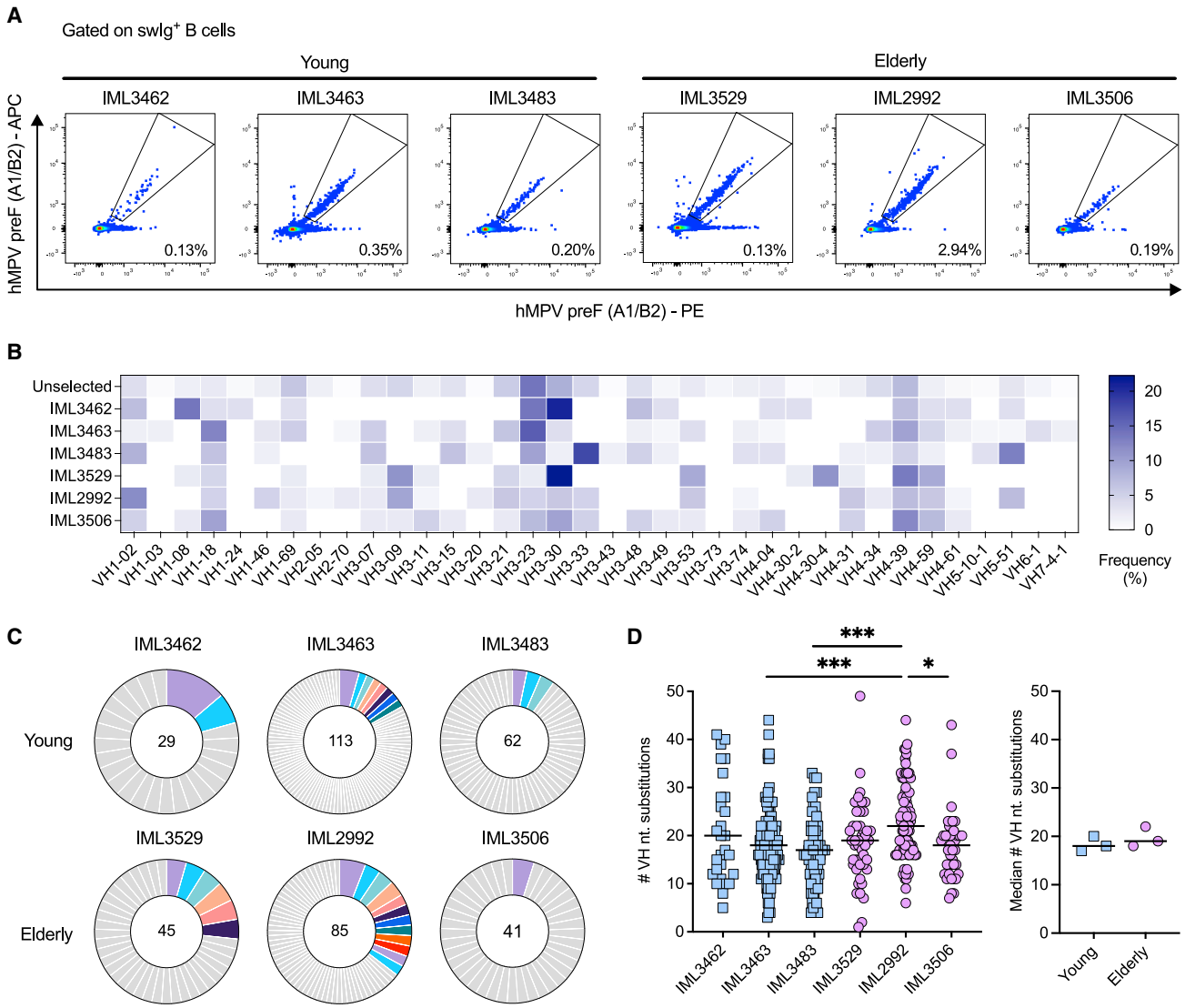

Figure 2. HMPV F-specific mAbs isolated from healthy donors possess diverse sequence features

(A) FACS strategy for the identification of hMPV preF-reactive swIg$^+$ B cells. The B cells shown in the gate were single-cell sorted for antibody cloning.

(B) VH germline gene usage among mAbs isolated from each donor, with matched frequencies from previously reported high-throughput sequencing of unselected human B cells (unselected) shown for comparison (Vander Heiden et al., 2017).

(C) Clonal lineage analysis. Each slice represents one clonal lineage, and the size of the slice is proportional to the number of clones in the lineage. Unique clones are shown in gray. The total number of clones is indicated in the center of the pie.

(D) Number of somatic nucleotide mutations in the VH-encoding region of mAbs isolated from each donor (left), and median SHM loads of mAbs from young and elderly donor repertoires (right). Black bars indicate medians. Statistical comparisons between donors were performed by two-sided Kruskal-Wallis tests with Dunn's correction for multiple comparisons, and comparisons between age cohorts were performed by two-sided Mann-Whitney U test. *$p < 0.05$; ***$p < 0.001$; swIg$^+$, class switched.

See also Table S2 and Figure S2.

(Figure 3D), which is consistent with the comparatively lesser sequence identity (~33%) between RSV and hMPV F (van den Hoogen et al., 2002), as well as the rarity of RSV/hMPV F cross-reactive MBCs (Figure 1E). Additionally, the hMPV/RSV cross-reactive mAbs displayed significantly higher SHM loads relative to hMPV F monospecific mAbs derived from the same donors (Figure 3E), potentially suggesting recruitment of cross-reactive B cells into secondary germinal centers following recurrent RSV and/or hMPV infections.

We next evaluated the mAbs for neutralizing activity against GFP-recombinant hMPV A1 isolate NL/1/00 to examine broad trends in neutralization among the isolated antibodies. Of the 375 mAbs that displayed binding activity to hMPV preF, 98 (26%) exhibited >80% neutralization of hMPV A1 at a concentration of 5 μg/mL, representing 17%–34% of each donor repertoire (Table S2; Figure 4A). Consistent with their similar binding affinities for hMPV preF A1 (Figure S3A), the mAbs derived from elderly and young adult donors displayed similar neutralization potencies

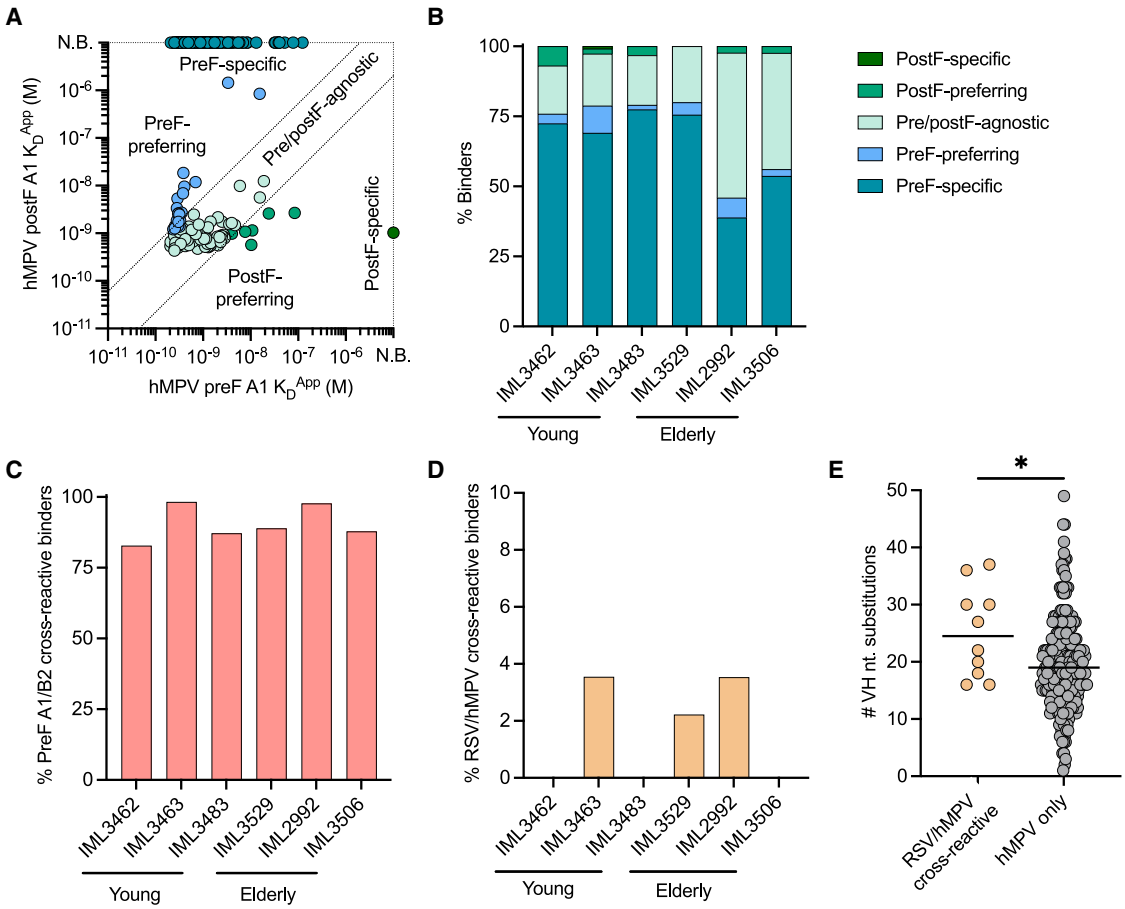

Figure 3. HMPV F-specific mAbs are predominantly preF-specific

(A) Apparent IgG-binding affinities for hMPV preF A1 and postF A1 proteins, as determined by BLI. MAbs that displayed a poor fit to a 1:1 binding model were excluded from this analysis. MAbs with preF and postF K_D^{App} differences greater than 4-fold were classified as preferential binders.

(B) Proportion of mAbs from each donor with the indicated binding profiles for hMPV preF and postF, as defined in (A).

(C and D) Proportion of hMPV preF A1/B2 (C) and hMPV/RSV preF (D) cross-reactive mAbs isolated from each donor, as assessed by BLI.

(E) Number of somatic nucleotide mutations in the VH-encoding region of RSV/hMPV F cross-reactive or hMPV F monospecific mAbs derived from donors with at least one RSV/hMPV F cross-reactive antibody. Black bars indicate medians. Neutralization assays were repeated twice across independent experiments. Statistical comparison was performed by two-sided Mann-Whitney U tests. *$p < 0.05$; K_D^{App}, apparent dissociation constant.

See also Table S2 and Figure S3.

(Figure 4A). As expected, the neutralizing antibodies displayed overall higher binding affinities for preF A1 relative to the poorly neutralizing and non-neutralizing antibodies (Figure S3B). However, 72% (170/236) of preF-specific mAbs displayed weak-to-undetectable neutralization of hMPV A1 at 5 μg/mL despite binding to hMPV preF A1 with high affinity (Figures 4B and 4C), suggesting recognition of cryptic epitopes that are partially or fully occluded in the context of the native hMPV F trimer. Furthermore, most neutralizing antibodies (73/98) bound to antigenic sites presented on both preF and postF (Figures 4B and S3C). Therefore, although preF-specific antibodies dominate the binding response to hMPV preF, these antibodies represent only a minor fraction of the neutralizing antibody response.

Rare hMPV F-specific antibodies demonstrate potent cross-subtype-neutralizing activity

To identify mAbs with broad and potent neutralizing activity, we performed titration studies on the 98 antibodies that displayed neutralizing activity against hMPV A1 in the initial screen. At a reduced concentration of 0.1 μg/mL, 30/98 mAbs retained >50% neutralizing activity against hMPV A1 (Table S2; Figure S3D). Titration of these 30 mAbs revealed half-maximal neutralization concentrations (neutralization IC_{50}s) ranging between 0.012 and 0.243 μg/mL (Table S2; Figure 4D). We next titrated these 30 neutralizing mAbs against hMPV A2, B1, and B2 isolates to determine their breadth of neutralization (Figure 4D). The vast majority of mAbs displayed similar neutralization potencies against hMPV A1 and A2 isolates TN/94/49 and SP/2/18 (Table S2; Figures 4D and 4E), which is consistent with the high degree of F protein identity between A1 and A2 subgroups (>98%) (Yang et al., 2009). In addition, all but four mAbs cross-neutralized hMPV B1 isolates NL/1/99 and SP/1/15, as well as B2 isolate NL/1/94, thereby demonstrating cross-subtype neutralization (Table S2; Figures 4D and 4E). B1 isolate NL/1/99 displayed significantly increased susceptibility to antibody neutralization compared with all other isolates tested,

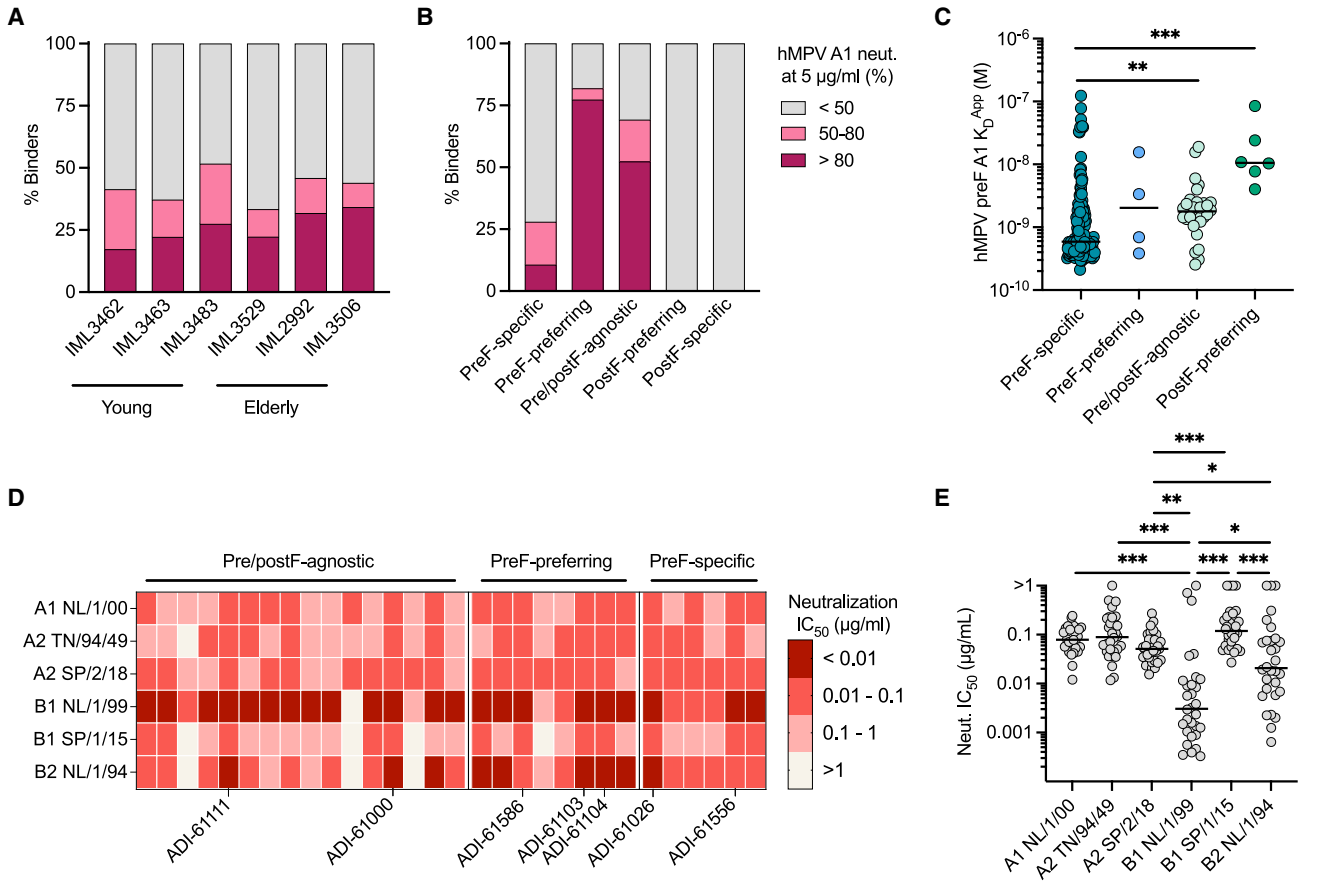

Figure 4. PostF cross-reactive mAbs drive the neutralizing antibody response to hMPV

(A and B) Proportion of mAbs with the indicated percent neutralization of GFP-recombinant hMPV A1 isolate NL/1/00 at a concentration of 5 µg/mL among hMPV F-specific mAbs isolated from each donor (A), or among mAbs with the indicated hMPV F-binding profiles (B).

(C) Apparent hMPV preF binding affinities of mAbs displaying <50% neutralization of hMPV A1 at a concentration of 5 µg/mL, grouped according to their hMPV F-binding profiles. Statistical comparisons were performed by two-sided Kruskal-Wallis tests with Dunn's correction for multiple comparisons.

(D) Heatmap of neutralization IC_{50}s against the indicated hMPV isolates for mAbs with >50% neutralization of hMPV A1 at a concentration of 0.1 µg/mL, grouped according to their hMPV F-binding profiles.

(E) Neutralization IC_{50}s against the indicated hMPV isolates for mAbs that displayed >50% neutralization of hMPV A1 at a concentration of 0.1 µg/mL. Black bars indicate medians. Statistical comparisons were performed by two-sided Friedman tests with Dunn's correction for multiple comparisons. *$p < 0.05$; **$p < 0.01$; ***$p < 0.001$; K_D^{App}, apparent dissociation constant.

See also Tables S2 and S3 and Figure S3.

including the B1 isolate SP/1/15 (Figure 4E), and this difference was observed with virus stocks generated in both Vero and Caco-2 cells (Figure S3E). In total, 7 mAbs exhibited broad and potent cross-subtype hMPV neutralization, with neutralization IC_{50}s < 0.1 µg/mL against all isolates tested (Table S3; Figure 4D). However, none of these antibodies displayed cross-reactivity with RSV F (Table S3), indicating that potently neutralizing hMPV/RSV cross-reactive antibodies are rarely elicited by natural infections.

Antibodies elicited by hMPV infection target 7 major antigenic sites

To define the antigenic sites targeted by the isolated mAbs, we performed competitive binding studies with a panel of high-affinity Fabs, a subset of which have been previously reported to target distinct epitopes on hMPV F (mAbs DS7, MPV458 and 234). We defined all hMPV epitopes in relation to analogous sites previously defined on RSV F (Graham, 2017; Huang et al., 2019). DS7 binds to an epitope within site I at the base of the F trimer (Wen et al., 2012); 234 binds the helix-loop-helix motif within site II (Ulbrandt et al., 2008); and MPV458 binds an epitope adjacent to site Ø at the trimer apex but partially within the interface between F protomers (Huang et al., 2020). RSV cross-reactive antibodies MPE8 and 101F, which bind conserved surfaces within sites III and IV, respectively (Corti et al., 2013; McLellan et al., 2010; Wen et al., 2017), were not included due to unsuitably fast off rates as Fabs (Figure S4A). Instead, we identified two RSV cross-reactive clones within our isolated set, ADI-61105 and ADI-61153, as high-affinity surrogates for MPE8 and 101F, respectively, based on their competitive binding profiles. Specifically, ADI-61105 competed with MPE8 IgG binding to both hMPV and RSV F but did not compete with the anti-RSV site II mAb motavizumab (Figures S4B and S4C). A negative-stain electron microscopy (nsEM) reconstruction of ADI-61105

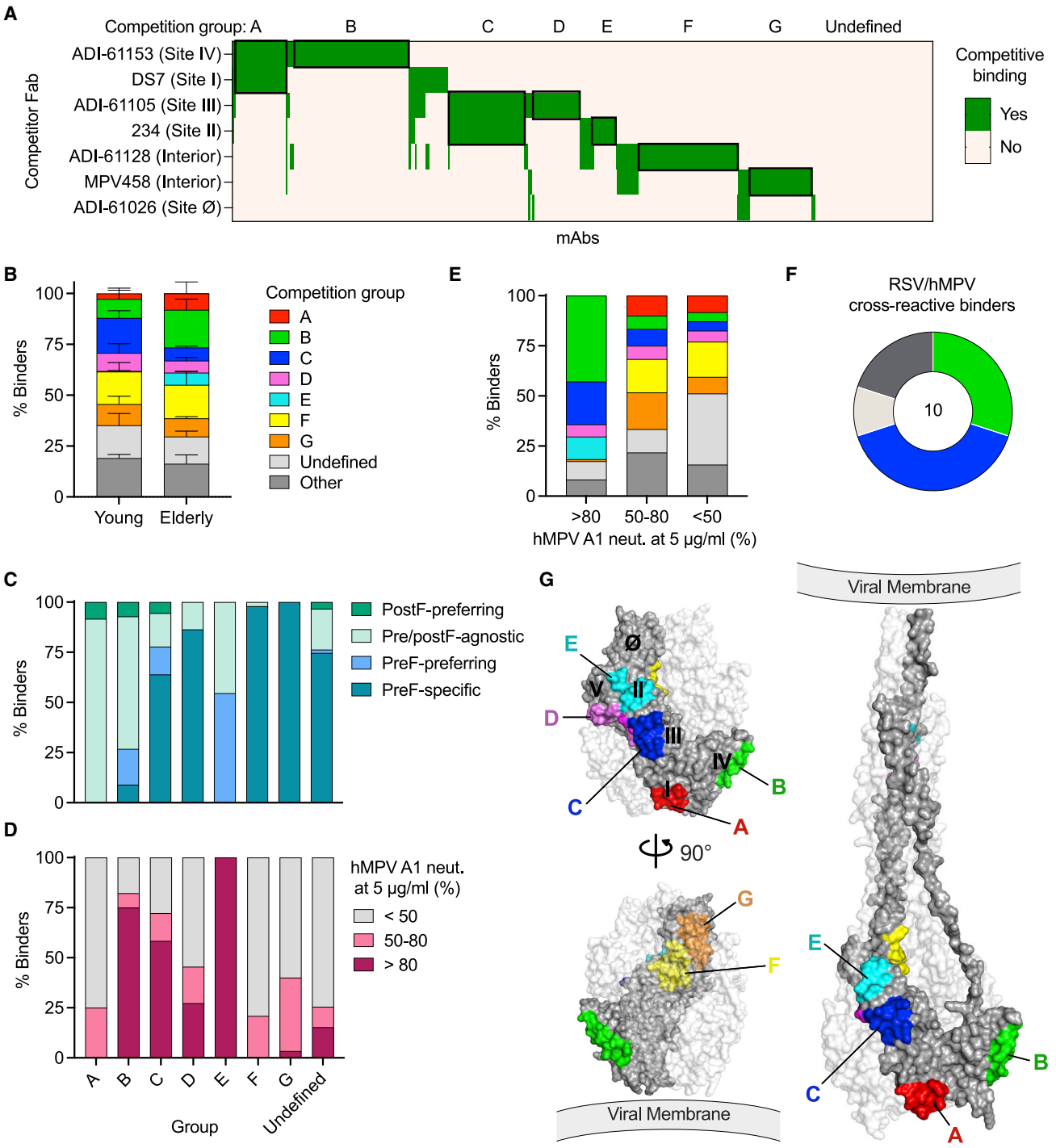

Figure 5. Antibodies elicited by hMPV infection target 7 major antigenic sites

(A) Analysis of mAb binding to hMPV preF A1 in the presence of the indicated competitor Fabs, relative to binding in the absence of competitor Fab, as assessed by flow cytometry. Competitor Fabs that resulted in greater than 4-fold reduced mAb binding were deemed competitive binders. MAbs were assigned to competition groups A–G based on their competitive binding profiles. MAbs that did not compete with any of the control Fabs are designated as "undefined."

(B) Mean proportions of mAbs that belong to the indicated competition groups among individual donor repertoires, grouped by donor age cohort. Error bars represent standard error of the mean. Statistical comparisons were performed by two-sided Mann-Whitney U tests with Bonferroni corrections for multiple comparisons.

(C and D) Proportion of mAbs within each competition group with the indicated hMPV F-binding profiles (C) or indicated percent neutralization of hMPV A1 (NL/1/00) at a concentration of 5 μg/mL (D).

(legend continued on next page)

Fab bound to hMPV F confirmed binding to a site III epitope partially overlapping that of MPE8 (Wen et al., 2017) but shifted toward the interprotomer interface and site V (Figure S4D). ADI-61153 competed for binding with 101F IgG and competed unidirectionally with DS7 (Figure S4B), suggesting that ADI-61153 binds an epitope within site IV that partially overlaps with site I.

Of the 375 isolated mAbs, 341 displayed sufficient affinity for hMPV preF A1 to be binned by Fab competition (Table S2; Figure 5A). 69% (234/341) of mAbs competed with one or more of the five mAbs described above. However, we found that an additional 14% (48/341) competed exclusively with ADI-61128, a weakly neutralizing preF-specific binder within our isolated set that did not compete with literature controls or their surrogates (Table S2; Figures 5A and S4B), suggesting that ADI-61128 binds a previously undefined but frequently targeted site on hMPV F. A 3D cryo-EM reconstruction of ADI-61128 Fab bound to hMPV F revealed that it binds an epitope deep within the trimer interior situated between site II and the MPV458 epitope (Figures S5A and S5B). Aligning the cryo-EM map with the hMPV F trimer in its closed conformation revealed that this epitope is only accessible via significant trimer breathing or dissociation into monomers (Figure S5C), as previously described for the binding of MPV458 (Huang et al., 2020).

In total, 282 mAbs competed with one or more of the 6 Fabs in our panel, revealing 7 distinct competition groups (designated as groups A–G) containing 10 or more members (Figure 5A). The proportion of antibodies targeting each antigenic site was similar across individual donors and the two age cohorts, suggesting that repeated exposures to hMPV and/or the process of immunosenescence do not substantially impact B cell immunodominance hierarchies for hMPV F (Figure 5B). In 3 out of 6 donors, group B, defined by competition with site IV mAb ADI-61153, was the dominant competition group, accounting for 20% (56/282) of binned mAbs (Figure 5B). Nearly all (91%) of these antibodies recognized both preF and postF and the majority (75%) displayed neutralizing activity at 5 μg/mL (Figures 5C and 5D). As such, a plurality of neutralizing antibodies (42/98) belonged to group B, including 3/7 potent cross-subtype neutralizers (Figure 5E; Table S3). In addition, 3/10 RSV cross-reactive mAbs were members of this competition group (Figure 5F). These results suggest that group B mAbs recognize epitopes within site IV that are expressed on both preF and postF, a subset of which target surfaces that are conserved between RSV and hMPV (Figure 5G; Battles et al., 2017; Más et al., 2016; McLellan et al., 2010; Mousa et al., 2018.

The remaining neutralizing mAbs primarily belonged to both groups C and E, defined by competition with site II mAb 234, with or without co-competition with site III mAb ADI-61105, respectively (Figures 5A and 5E). Together, 33% (32/98) of neutralizers and 2/7 potent cross-subtype neutralizers targeted these antigenic sites (Figure 5E; Table S3). Although only a small set of mAbs belonged to group E (11/282), each mAb in this group reacted with both preF and postF and displayed neutralizing activity in the initial screen (Figures 5C and 5D). These results suggest the recognition of antigen site II (Figure 5G). In contrast, 64% (23/36) of mAbs in group C were preF specific (Figure 5C), and despite the overall poor neutralization of preF-specific binders (Figure 4B), 48% (11/23) of group C mAbs were neutralizing (Figure 5D). Group C also contained the largest subset (4/10) of RSV cross-reactive mAbs (Figure 5F). These data suggest that mAbs in group C primarily bind site III (Figure 5G), which is highly conserved between hMPV and RSV F and has been previously shown to be targeted by neutralizing preF-specific mAbs (Corti et al., 2013; Gilman et al., 2016; Wen et al., 2017).

The majority of mAbs in each of the remaining groups (A, D, F, and G) displayed little-to-no neutralizing activity against hMPV A1 (Figure 5D). Combined, these groups accounted for 44% (124/282) of binned mAbs but only 7% (7/98) of neutralizers (Figures 5A and 5E). While mAbs in group A had poor affinity for hMPV preF A1, mAbs in groups D, F, and G exhibited high affinity to hMPV preF A1 and were predominately or exclusively preF-specific (Table S2; Figure 5C). These largely preF-specific and poorly neutralizing mAbs displayed competitive binding with Fabs (ADI-61105, ADI-61128, or MPV458) that bind either partially or entirely within the trimer interior (Figures 5A, 5G, S4D, and S5). Therefore, the poor neutralization of these mAbs is likely due to recognition of cryptic epitopes that are poorly accessible in the context of the native hMPV F trimer. Altogether, our results show that antibody neutralization of hMPV is highly epitope dependent, with mAbs targeting epitopes expressed on both preF and postF dominating the neutralizing antibody response.

ADI-61026 binds a site of vulnerability near the F trimer apex

While most (42/44) preF-specific mAbs with undefined binding sites displayed poor neutralizing activity (Table S2; Figures 5C and 5D), ADI-61026 potently neutralized all hMPV isolates tested (Figure 4D, Table S3). Competitive binding studies with ADI-61026 revealed that only 10/341 mAbs bound to epitopes overlapping its binding site, of which 8 also competed with MPV458 (7/8) and/or ADI-61105 (2/8) (Table S2; Figure 5A). Notably, no other potently neutralizing antibodies competed with ADI-61026 (Table S3). These data suggest that ADI-61026 recognizes a rarely targeted site of vulnerability adjacent to the MPV458 epitope near the F trimer apex.

To structurally define the epitope bound by ADI-61026, we determined a cryo-EM structure of ADI-61026 and MPE8 Fabs

(E and F) Competition groups of mAbs displaying the indicated percent neutralization of hMPV A1 at a concentration of 5 μg/mL (E) or that cross-react with both hMPV and RSV F, as assessed by BLI (F).

(G) Inferred antigenic sites targeted by mAbs belonging to each competition group based on known epitopes of control mAbs used for binning, colored by competition group and mapped onto a single protomer of hMPV preF (left, PDB: 5WB0) or postF (right, PDB: 5L1X). Antigenic sites are labeled in relation to analogous sites previously defined on RSV F (Graham, 2017; Huang et al., 2019). Additional protomers of trimeric hMPV F are shown in transparency. MAbs that did not display sufficient binding to hMPV preF A1 for competition binning were excluded from all analyses. Competitive binding analyses were repeated across two independent experiments.

See also Table S2 and Figures S4 and S5.

complexed with hMPV F. The initial 3D reconstruction from 113,336 particles yielded a global resolution of 3.5 Å (Figures S6A and S6B). The EM map showed full occupancy of ADI-61026 Fab bound to antigenic site Ø, near the trimer apex (Figures 6A and 6B). As expected, MPE8 Fab spanned antigenic sites II, III, and V, as well as site IV from neighboring protomers, stabilizing the F trimer (Wen et al., 2017). We next performed a local refinement focusing on the ADI-61026 Fab-binding site, generating improved resolution of the binding interface for model building (Figures 6C and S6C–S6F). Overall, the heavy and light chains of ADI-61026 engage both subunits of F (F_1 and F_2) via polar and hydrophobic interactions, burying a combined 649 $Å^2$ of surface area (Figure 6D).

The heavy chain of ADI-61026 primarily contacts the base of site Ø, with all three complementarity-determining regions (CDRs) contributing to the binding interface (Figure 6D). In contrast, the light chain primarily packs against the apex of site Ø, with the L-CDR1 and L-CDR2 contacting the loop preceding the α4 helix of the F_1 subunit. The most prominent interaction between ADI-61026 and the F trimer is the insertion of Trp100 from the H-CDR3 into a hydrophobic pocket formed by Leu58 and Leu71 from F_2 and Leu173 and Ile177 from F_1 (Figure 6D). In addition, polar interactions are observed at each residue flanking Trp100; Asp99 forms hydrogen bonds with Thr59 from F_2 and Asn180 from F_1, and Lys100a forms a salt bridge with Asp54 from F_2. Notably, the side chain of Ser32 in the H-CDR1 interacts with the N-glycan at Asn57, which is one of two N-glycans at site Ø (Figure 6D). In addition, Glu54 in the H-CDR2 forms a salt bridge with Lys166 in the α4 helix of the F_1 subunit. The light-chain interactions with hMPV F center on Lys179 from F_1, reaching out from the trimer apex to form polar interactions with Tyr32 in the L-CDR1, Asp51 in the L-CDR2, and Ser66 in the framework region preceding the L-CDR3 (Figures 6C and 6D).

Alignment of the F protein sequences of the tested hMPV isolates revealed a high degree of amino acid conservation within the ADI-61026 epitope (Figure 6E), with only Lys175 and Lys179 varying between isolates and only Lys179 making direct contacts with ADI-61026 Fab (Figure 6D). Modeling the K179R mutation observed in B1 isolates into our hMPV F-ADI-61026 structure revealed that Arg179 likely maintains each of the polar interactions formed by Lys179 (Figure 6D), providing a molecular explanation for the observed broad cross-subtype neutralization of ADI-61026. Modeling N-linked glycans onto the structure of hMPV F bound by ADI-61026 Fab (Bohne-Lang and von der Lieth, 2005) revealed that the ADI-61026 epitope is situated directly between branched glycans originating from Asn57 and Asn172 (Figure S7A), providing a molecular explanation for the ability of this mAb to penetrate the dense glycan shield at the apex of the pre-fusion F trimer. Furthermore, the modeled glycan originating from Asn172 overlaps with ADI-61026 Fab bound to adjacent protomers, suggesting that glycan flexibility may be required for the binding of multiple ADI-61026 molecules.

Mapping the ADI-61026 epitope onto the structure of hMPV postF (PDB: 5L1X) shows its complete disruption (Figure S7B), providing a structural explanation for the preF specificity of this mAb. MPV458 is the only structurally defined hMPV F antibody that binds in the vicinity of the ADI-61026 epitope (Figure S7C; Huang et al., 2020). Although both antibodies contact the N-glycan at Asn57, they bind with distinct angles of approach (Figure S7C) and therefore do not compete for binding (Figure 7A). In addition, two potently neutralizing RSV antibodies, D25 and AM22, that recognize either the loop preceding the α1 helix in F_2 or the α4 helix in F_1 of RSV (Jones et al., 2019; McLellan et al., 2013b) bind highly similar epitopes to that of ADI-61026 on hMPV F (Figure S7D). Collectively, we identified a rare, highly potent broadly neutralizing preF-specific antibody that targets a site of vulnerability at antigenic site Ø near the hMPV F trimer apex.

Potently neutralizing antibodies targeting three distinct antigenic sites protect *in vivo*

To investigate the relationship between hMPV *in vitro* neutralization and *in vivo* protection, we selected three mAbs (ADI-61026, ADI-61104, and ADI-61556) for evaluation in passive transfer and challenge experiments in a cotton rat model as monotherapies. Each of these mAbs were potently neutralizing across virus subgroups, with neutralization IC_{50} values below 0.1 μg/mL against all hMPV isolates tested (Figure 4D, Table S3). They also recognized mutually exclusive epitopes on hMPV F: ADI-61026 targets site Ø (Figure 6); ADI-61104 binds to an epitope overlapping that of the site I mAb DS7 and the site III mAb MPE8; and ADI-61556 recognizes an epitope spanning sites II and III (Figure 7A). Cotton rats were dosed by intramuscular injection with 1 mg/kg of anti-hMPV IgGs or an irrelevant anti-HEL isotype control (ADI-26140) 24 h prior to intranasal challenge with 10^5 plaque-forming units (PFUs) of hMPV A2 isolate TN/94/49 (Figure 7B). This dose was calculated to yield serum-neutralizing antibody titers at the time of challenge between 1:100 and 1:1,000, which are associated with prophylactic protection against other viral infections including RSV, HIV, and SARS-CoV-2 (Rogers et al., 2020; Sok and Burton, 2018; Zhu et al., 2017). For rats dosed with anti-hMPV mAbs, median serum-neutralizing titers at the time of challenge ranged from 1:103 to 1:636 and reflected the neutralization potencies of the three mAbs (Table S3; Figure 7C).

4 days following challenge, the rats were sacrificed, and their lung and nasal tissues were collected for viral load analysis (Figure 7B). Animals in the three groups that received the potently neutralizing anti-hMPV mAbs had 10- to 20-fold fewer copies of hMPV mRNA in their lungs following challenge and lung viral titers uniformly below the lower limit of detection (Figures 7D and 7E). However, only animals treated with ADI-61026 or ADI-61556 displayed significant reductions in viral replication in the nose (Figure 7F). Cotton rats treated with ADI-61104 failed to show a significant reduction in nasal viral titers despite exhibiting similar serum-neutralizing titers to rats treated with ADI-61026 or ADI-61556 at the time of challenge, suggesting that the epitope targeted by anti-hMPV mAbs may impact their protective efficacy in the upper airway (Figures 7C and 7F). We conclude that potently neutralizing antibodies isolated from naturally infected adult donors can provide robust prophylactic protection against hMPV infection in a small animal model.

DISCUSSION

A comprehensive understanding of the human MBC response to natural hMPV infection will facilitate the development of hMPV vaccines and immunotherapeutics. Although previous studies have coarsely defined the epitopes targeted by anti-hMPV-F

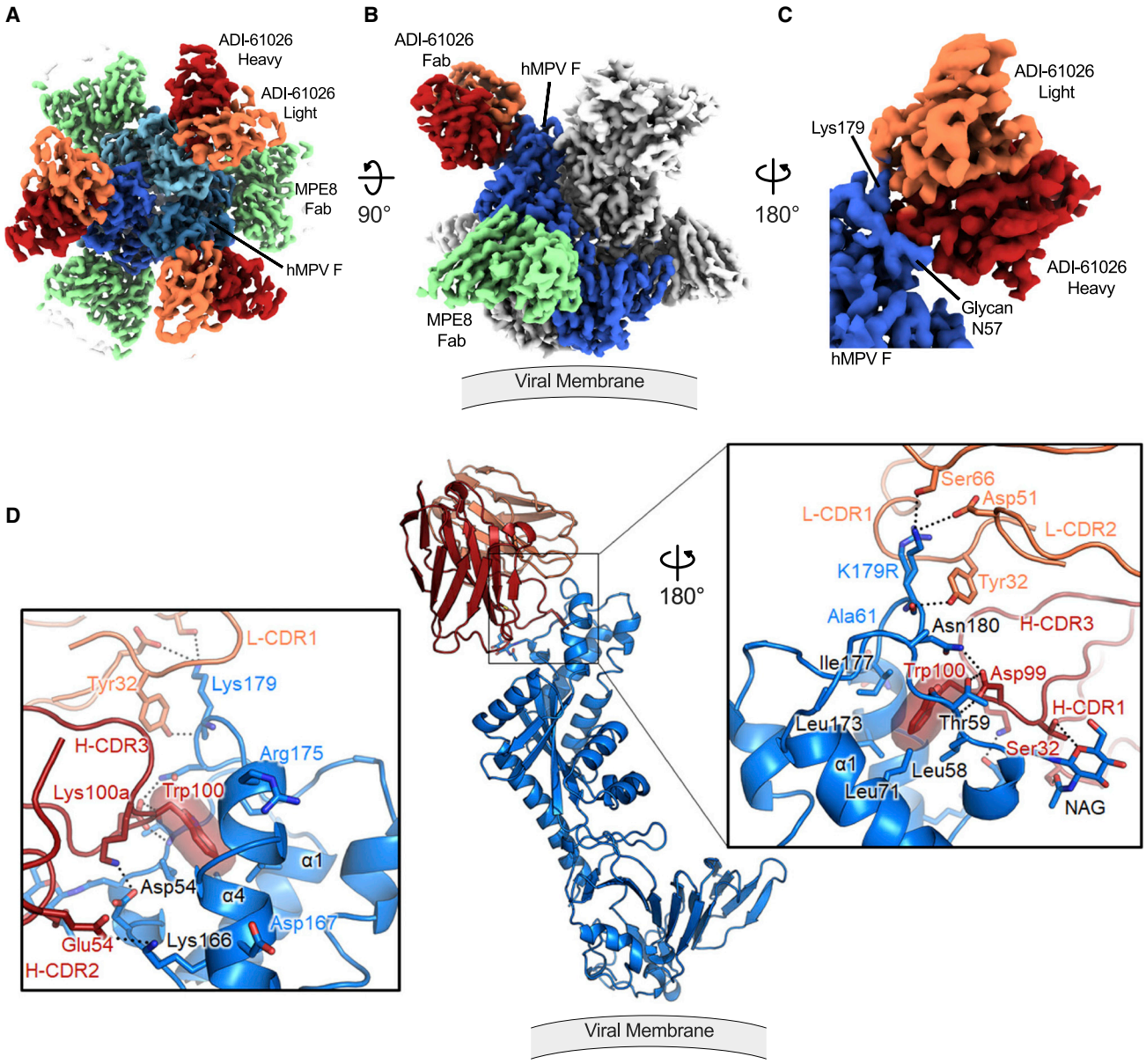

E

		53	54			57	58	59	60											71		73
A	A1 NL/1/00	G	D	V	E	N	L	T	C	A	D	G	P	S	L	I	K	T	E	L	D	L
	A2 TN/94/49	G	D	V	E	N	L	T	C	A	D	G	P	S	L	I	K	T	E	L	E	L
	A2 SP/2/18	G	D	V	E	N	L	T	C	A	D	G	P	S	L	I	K	T	E	L	D	L
B	B1 NL/1/99	G	D	V	E	N	L	T	C	T	D	G	P	S	L	I	K	T	E	L	D	L
	B1 SP/1/15	G	D	V	E	N	L	T	C	T	D	G	P	S	L	I	K	T	E	L	D	L
	B2 NL/1/94	G	D	V	E	N	L	T	C	T	D	G	P	S	L	I	K	T	E	L	D	L

	165	166							173	174	175		177	178	179	180		182	183
A1 NL/1/00	L	K	D	F	V	S	K	N	L	T	R	A	I	N	K	N	K	C	D
A2 TN/94/49	L	K	D	F	V	S	K	N	L	T	R	A	I	N	K	N	K	C	D
A2 SP/2/18	L	K	D	F	V	S	K	N	L	T	R	A	I	N	K	N	K	C	D
B1 NL/1/99	L	K	E	F	V	S	K	N	L	T	S	A	I	N	R	N	K	C	D
B1 SP/1/15	L	K	E	F	V	S	K	N	L	T	S	A	I	N	R	N	K	C	D
B2 NL/1/94	L	K	E	F	V	S	K	N	L	T	S	A	I	N	K	N	K	C	D

Figure 6. ADI-61026 binds a site of vulnerability near the F trimer apex

(A) Top view of cryo-EM map of ADI-61026 and MPE8 Fabs bound to hMPV preF. F protomers are shown in shades of blue. The heavy chain of ADI-61026 is colored red, and the light chain is colored coral. MPE8 Fab is shown in green.

(B) Side view of the ADI-61026-MPE8-F complex. One Fab-bound protomer is colored as in (A), and the remainder are shown in white or gray.

(C) Focused map of ADI-61026 Fab bound to a hMPV F protomer, with key residues indicated.

(D) Atomic model of the ADI-61026-F complex depicted as ribbons, with zoomed views of the binding interface shown from two angles, and key interacting residues displayed as sticks. The K179R mutation in hMPV F is modeled to show the conservation of polar interactions. Oxygen atoms are colored red, and nitrogen atoms are colored blue. Hydrogen bonds and salt bridges are depicted as black dotted lines. NAG, N-acetyl glucosamine.

(E) Sequence conservation of the ADI-61026 epitope across the indicated hMPV A and B isolates. Residues are shaded by their degree of conservation among the indicated isolates, and residues within 5 Å of the ADI-61026 Fab are highlighted in red.

See also Table S4 and Figures S6 and S7.

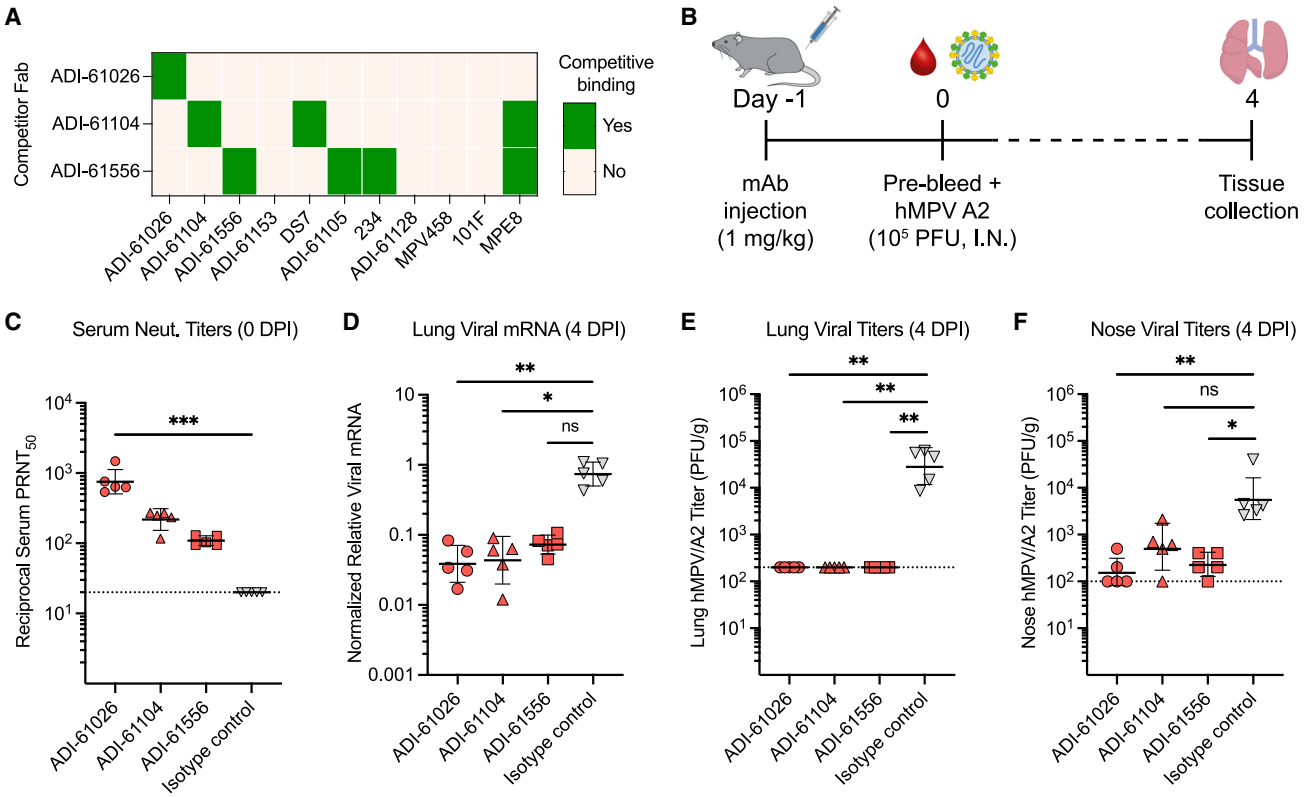

Figure 7. Three potently neutralizing mAbs protect in a cotton rat model of hMPV infection

(A) Competitive binding profiles of mAbs selected for protection studies. Competitor Fabs that resulted in greater than 4-fold mAb reduced binding relative to binding in the absence of competitor Fab, as assessed by flow cytometry, were deemed competitive binders.

(B) HMPV F-specific neutralizing IgGs or a control anti-HEL IgG were administered intramuscularly at a dose of 1 mg/kg (n = 5 animals per group) 24 h prior to intranasal challenge with 10^5 PFU of hMPV A2 (TN/94/49). Serum was collected immediately prior to challenge (day 0). On day 4 post-challenge, lung and nasal tissues were resected for viral titer assessment.

(C) Half-maximal plaque-reduction neutralizing titers ($PRNT_{50}$) of cotton rat sera at the time of challenge.

(D) HMPV L polymerase mRNA copies in lung homogenates collected 4 days post-hMPV A2 challenge, as assessed by quantitative PCR (qPCR).

(E and F) Endpoint-dilution viral titers in lung (E) or nasal tissue (F) homogenates collected 4 days post-hMPV A2 challenge. Black bars indicate geometric means, error bars indicate geometric standard deviations, and dashed lines indicate lower limits of detection. Competition binning analyses were repeated across two independent experiments. Animal challenge experiments were not repeated. Statistical comparisons were performed by two-sided Kruskal-Wallis tests with Dunn's correction for multiple comparisons. *p < 0.05; **p < 0.01; ***p < 0.001; ns, not significant; I.N., intranasal; PFU, plaque-forming unit.

serum antibodies, the frequencies, fine specificities, and functional properties of antibodies encoded by hMPV F-specific MBCs have remained undefined. Here, we deeply mined the hMPV preF-reactive MBC repertoires of both elderly and young adult donors and isolated a panel of potent cross-subtype neutralizing antibodies that target several distinct sites of vulnerability on the hMPV F trimer, including a site of vulnerability at the pre-fusion F trimer apex. The three most potent mAbs each afforded robust protection against lower respiratory tract infection in a small animal model of hMPV infection.

Because severe hMPV disease disproportionately impacts the elderly (Falsey et al., 2003; Haas et al., 2013; Shafagati and Williams, 2018), we compared MBC responses with hMPV F between elderly and young adult donor cohorts. We found that the sequence features, binding affinities, epitope specificities, and functional properties of hMPV F-specific antibodies isolated from young adult and elderly donors were highly similar, suggesting that the process of immunosenescence and the accumulation of additional hMPV infections in elderly individuals may not substantially impact their hMPV F-specific MBC repertoire. This contrasts with previous studies of influenza, which have shown that vaccine-induced plasmablast responses in elderly individuals are significantly less clonally diverse and have a reduced accumulation of *de novo* somatic mutations compared with young adults (de Bourcy et al., 2017; Henry et al., 2019). Given that our study focused on MBC repertoires, this discrepancy may suggest that immunosenescence impacts recall and *de novo* responses induced by secondary viral exposures but does not collapse the pre-existing diversity within the MBC compartment. Alternatively, this difference may be driven by the increased genetic variability of influenza compared with hMPV, thus providing greater opportunities for the induction of *de novo* responses following repeated exposures.

Consistent with previous serum-mapping studies (Battles et al., 2017; Huang et al., 2021), we found that the majority of neutralizing antibodies induced by natural hMPV infection are directed to epitopes expressed on both preF and postF. Competitive binding studies further revealed that these antibodies largely

target epitopes analogous to antigenic sites II, III, and IV on RSV F. In contrast, potently neutralizing antibodies to RSV primarily recognize preF-specific antigenic sites Ø and V near the trimer apex (Gilman et al., 2016). The scarcity of preF-specific neutralizing specificities within hMPV F-specific MBC repertoires is likely due to glycan shielding of analogous sites on the hMPV F trimer (Battles et al., 2017). Nevertheless, we identified and structurally characterized a rare, highly potent preF-specific antibody, ADI-61026, that breaches this glycan shield to bind a site Ø epitope at the apex of the hMPV F trimer. This interaction is centered around the insertion of a large hydrophobic sidechain from the H-CDR3 of ADI-61026 into a deep pocket formed by both subunits of F situated directly between the two N-glycans in site Ø. ADI-61026 also directly interacts with the N-glycan at Asp57 via a germline-encoded residue in its H-CDR1. However, the VH2-70 germline gene utilized by this antibody is infrequently represented in human B cell repertoires (~0.25%) (Vander Heiden et al., 2017), which may account in part for the rarity of this class of potently neutralizing hMPV antibodies.

In contrast to the potent neutralization observed for ADI-61026, the vast majority of preF-specific hMPV antibodies were non-neutralizing and targeted cryptic trimer-internal epitopes, suggesting that these commonly targeted sites may not be readily accessible in the context of the native hMPV F trimer. While molecular breathing of hMPV F has been previously suggested in the context of MPV458 binding (Huang et al., 2020), we discovered a class of trimer-internal binders typified by ADI-61128 that may suggest that hMPV F possesses even greater flexibility in its pre-fusion conformation than previously believed. While MPV458 binds an epitope partially within the trimer interface near the apex of the pre-fusion F trimer, ADI-61128 binds a more basal epitope deep within the trimer interior. Notably, RSV antibodies targeting analogous preF-specific cryptic epitopes have not been described to date, which may be due to more limited molecular breathing of RSV F and/or the nature of the stabilized RSV F antigens used for B cell isolation (Gilman et al., 2016). More limited exposure of trimer-internal non-neutralizing sites may also explain the improved vaccine-induced neutralizing antibody responses elicited by engineered hMPV preF antigens stabilized with interprotomer disulfide bonds (Stewart-Jones et al., 2021) or improved interprotomer electrostatic interactions (Hsieh et al., 2022). Our structural studies of hMPV preF-specific non-neutralizing antibodies directed to the trimer interior and potently neutralizing antibodies directed to the trimer apex may enable further engineering of preF-based immunogens that preferentially induce neutralizing antibody responses.

Lastly, given the clinical successes of the mAbs palivizumab and nirsevimab in the prevention of severe RSV disease in high-risk infants (The IMpact-RSV Study Group, 1998; Hammitt et al., 2022), we evaluated three highly potent cross-subtype neutralizing antibodies for their ability to protect against hMPV infection in a small animal model. In a pre-exposure prophylaxis setting, each of these mAbs provided significant protection against hMPV infection in the lower respiratory tract, and two out of the three antibodies also provided significant protection against upper respiratory tract infection. As neutralizing antibody titers are the primary correlate of protection from viral replication in the nose in the context of the related respiratory virus RSV (Zohar et al., 2022), increased dosages of these potently neutralizing hMPV antibodies may provide increased protection against upper respiratory tract infection. In addition, as Fc-effector functions can contribute to protection from RSV, including in cotton rat models (Hiatt et al., 2014; van Erp et al., 2019; Zohar et al., 2022), it is possible that Fc-effector mechanisms may have contributed to the protection conferred by our potently neutralizing hMPV antibodies. Lastly, since these three mAbs recognize non-overlapping epitopes, they could be combined to mitigate the emergence of resistant variants, as previously described in the context of ebolavirus, HIV, and SARS-CoV-2 (Baum et al., 2020; Saphire et al., 2018; Walsh and Seaman, 2021). Altogether, this study provides fundamental insights into the human B cell response elicited by natural hMPV infection, which may facilitate the design and evaluation of hMPV preF-based vaccines that induce protective antibody responses. Furthermore, the potent and protective neutralizing antibodies described herein represent promising candidates for mAb prophylaxis.

Limitations of the study

A limitation of our anti-hMPV F repertoire analysis is the relatively small number of donors studied. However, the high degree of similarity among the donor repertoires studied combined with the overall agreement of our findings with previously published serum-mapping studies (Battles et al., 2017; Huang et al., 2021) suggest that the characteristics of the antibody repertoires described here are likely representative of most naturally infected human donors.

It is unknown to what extent the MBC repertoires describe here reflect the composition of the serum antibody repertoire, which is maintained by long-lived plasma cells residing in the bone marrow. Future studies using emerging serum proteomics technologies (Ionov and Lee, 2022) will be required to investigate this question.

STAR★METHODS

Detailed methods are provided in the online version of this paper and include the following:

- KEY RESOURCES TABLE
- RESOURCE AVAILABILITY
  - Lead contact
  - Materials availability
  - Data and code availability
- EXPERIMENTAL MODEL AND SUBJECT DETAILS
  - Human subjects
  - Animal studies
  - Cell lines
- METHOD DETAILS
  - hMPV and RSV antigens
  - Enzyme-linked immunosorbent assays
  - Memory B cell staining and single B cell sorting
  - Amplification and cloning of antibody variable genes
  - Expression and purification of IgG and Fab
  - BLI kinetic measurements
  - Competition analysis using BLI
  - Competitive binning
  - *In vitro* neutralization assays
  - Cotton rat challenge model

- Viral titration of lung and nose homogenates
- Viral mRNA quantitation
- Cryo-EM sample preparation and data collection
- Cryo-EM data processing
- Negative stain electron microscopy

● QUANTIFICATION AND STATISTICAL ANALYSIS

SUPPLEMENTAL INFORMATION

Supplemental information can be found online at https://doi.org/10.1016/j.immuni.2022.07.003.

ACKNOWLEDGMENTS

We thank C. Williams for assistance with figure preparation; and E. Krauland, J. Nett, M. Vásquez, and M. Battles for helpful comments on the manuscript. All IgGs were sequenced by Adimab's Molecular Core and produced by the High Throughput Expression group. BLI binding and competition experiments were performed by Adimab's protein analytics group. We thank B. van den Hoogen and R. Fouchier for providing GFP-recombinant viruses of hMPV isolates A1 NL/1/00 and B1 NL/1/99 and non-recombinant hMPV isolate B2 NL/1/94. We thank Dr. Inmaculada Casas (Instituto de Salud Carlos III) for providing hMPV isolates A2 SP/2/18 and B1 SP/1/15. We acknowledge the Immune Monitoring and Flow Cytometry Resource (IMFCSR) at the Norris Cotton Cancer Center at Dartmouth supported by NCI Cancer Center Support Grant 5P30 CA023108-41. We thank Dr. John Ludes-Meyers and Dr. Kaci Erwin for technical assistance. We acknowledge the University of Texas College of Natural Sciences and award RR160023 of the Cancer Prevention and Research Institute of Texas for support of the EM facility at the University of Texas at Austin. This work was funded in part by Welch Foundation grant number F-0003-19620604. We also thank K. Yim and Sigmovir Biosystems, Inc for conducting all hMPV A2 neutralization and protection studies.

AUTHOR CONTRIBUTIONS

L.M.W. and J.S.M. conceived and designed the study. C.G.R., J.C.G., A.Z.W., and M.S. performed flow cytometric analyses and single-cell cloning. C.G.R. and E.S.E. conducted serum ELISA and competition binning experiments. C.-L.H., S.A.R., and J.S.M. designed and produced the hMPV and RSV antigens and performed structural characterizations. T.D. and V.M. conducted and analyzed hMPV neutralization assays. C.G.R., C.-L.H., S.A.R., and E.S.E. wrote the manuscript, and all authors reviewed and edited the manuscript.

DECLARATION OF INTERESTS

C.G.R., E.S.E., J.C.G., A.Z.W., M.S., and L.M.W. are current or former employees of Adimab, LLC and may hold shares in Adimab, LLC. L.M.W. is an employee of Adagio Therapeutics Inc. and holds shares in Adagio Therapeutics Inc.

Received: January 20, 2022
Revised: May 16, 2022
Accepted: July 6, 2022
Published: August 8, 2022

REFERENCES

Adams, P.D., Afonine, P.V., Bunkóczi, G., Chen, V.B., Davis, I.W., Echols, N., Headd, J.J., Hung, L.W., Kapral, G.J., Grosse-Kunstleve, R.W., et al. (2010). Phenix: a comprehensive Python-based system for macromolecular structure solution. Acta Crystallogr. D Biol. Crystallogr. *66*, 213–221. https://doi.org/10.1107/S0907444909052925.

Afonso, C.L., Amarasinghe, G.K., Bányai, K., Bào, Y., Basler, C.F., Bavari, S., Bejerman, N., Blasdell, K.R., Briand, F.X., Briese, T., et al. (2016). Taxonomy of the order Mononegavirales: update 2016. Arch. Virol. *161*, 2351–2360. https://doi.org/10.1007/s00705-016-2880-1.

Aliprantis, A.O., Wolford, D., Caro, L., Maas, B.M., Ma, H., Montgomery, D.L., Sterling, L.M., Hunt, A., Cox, K.S., Vora, K.A., et al. (2021). A Phase 1 randomized, double-blind, placebo-controlled trial to assess the safety, tolerability, and pharmacokinetics of a respiratory syncytial virus neutralizing monoclonal antibody MK-1654 in healthy adults. Clin. Pharmacol. Drug Dev. *10*, 556–566. https://doi.org/10.1002/cpdd.883.

Anderson, E.J., Simões, E.A., Buttery, J.P., Dennehy, P.H., Domachowske, J.B., Jensen, K., Lieberman, J.M., Losonsky, G.A., and Yogev, R. (2012). Prevalence and characteristics of human Metapneumovirus infection Among hospitalized children at high risk for severe lower respiratory tract infection. J. Pediatr. Infect. Dis. Soc. *1*, 212–222. https://doi.org/10.1093/jpids/pis069.

Bar-Peled, Y., Diaz, D., Pena-Briseno, A., Murray, J., Huang, J., Tripp, R.A., and Mousa, J.J. (2019). A potent neutralizing site III-specific human antibody neutralizes human Metapneumovirus in vivo. J. Virol. *93*. https://doi.org/10.1128/JVI.00342-19.

Battles, M.B., Más, V., Olmedillas, E., Cano, O., Vázquez, M., Rodríguez, L., Melero, J.A., and McLellan, J.S. (2017). Structure and immunogenicity of pre-fusion-stabilized human Metapneumovirus F glycoprotein. Nat. Commun. *8*, 1528. https://doi.org/10.1038/s41467-017-01708-9.

Baum, A., Fulton, B.O., Wloga, E., Copin, R., Pascal, K.E., Russo, V., Giordano, S., Lanza, K., Negron, N., Ni, M., et al. (2020). Antibody cocktail to SARS-CoV-2 spike protein prevents rapid mutational escape seen with individual antibodies. Science *369*, 1014–1018. https://doi.org/10.1126/science.abd0831.

Bohne-Lang, A., and von der Lieth, C.W. (2005). GlyProt: in silico glycosylation of proteins. Nucleic Acids Res. *33*, W214–W219. https://doi.org/10.1093/nar/gki385.

Casañal, A., Lohkamp, B., and Emsley, P. (2020). Current developments in coot for macromolecular model building of Electron Cryo-microscopy and Crystallographic Data. Protein Sci. *29*, 1069–1078. https://doi.org/10.1002/pro.3791.

Corti, D., Bianchi, S., Vanzetta, F., Minola, A., Perez, L., Agatic, G., Guarino, B., Silacci, C., Marcandalli, J., Marsland, B.J., et al. (2013). Cross-neutralization of four paramyxoviruses by a human monoclonal antibody. Nature *501*, 439–443. https://doi.org/10.1038/nature12442.

Croll, T.I. (2018). Isolde: a physically realistic environment for model building into low-resolution electron-density maps. Acta Crystallogr. D Struct. Biol. *74*, 519–530. https://doi.org/10.1107/S2059798318002425.

de Bourcy, C.F., Angel, C.J., Vollmers, C., Dekker, C.L., Davis, M.M., and Quake, S.R. (2017). Phylogenetic analysis of the human antibody repertoire reveals quantitative signatures of immune senescence and aging. Proc. Natl. Acad. Sci. USA *114*, 1105–1110. https://doi.org/10.1073/pnas.1617959114.

de Graaf, M., Herfst, S., Schrauwen, E.J., van den Hoogen, B.G., Osterhaus, A.D., and Fouchier, R.A. (2007). An improved plaque reduction virus neutralization assay for human Metapneumovirus. J. Virol. Methods *143*, 169–174. https://doi.org/10.1016/j.jviromet.2007.03.005.

Dunbar, J., Krawczyk, K., Leem, J., Marks, C., Nowak, J., Regep, C., Georges, G., Kelm, S., Popovic, B., and Deane, C.M. (2016). SAbPred: a structure-based antibody prediction server. Nucleic Acids Res. *44*, W474–W478. https://doi.org/10.1093/nar/gkw361.

Edwards, K.M., Zhu, Y., Griffin, M.R., Weinberg, G.A., Hall, C.B., Szilagyi, P.G., Staat, M.A., Iwane, M., Prill, M.M., and Williams, J.V.; New Vaccine Surveillance (2013). Burden of human Metapneumovirus infection in young children. N. Engl. J. Med. *368*, 633–643. https://doi.org/10.1056/NEJMoa1204630.

Evans, R.O.N.,M., Pritzel, A., Antropova, N., Senior, A., Green, T., Žídek, A., Bates, R., Blackwell, S., Yim, J., et al. (2022). Protein complex prediction with AlphaFold-Multimer. Preprint at bioRxiv. https://doi.org/10.1101/2021.10.04.463034.

Falsey, A.R., Erdman, D., Anderson, L.J., and Walsh, E.E. (2003). Human Metapneumovirus infections in young and elderly adults. J. Infect. Dis. *187*, 785–790. https://doi.org/10.1086/367901.

Fels, J.M., Maurer, D.P., Herbert, A.S., Wirchnianski, A.S., Vergnolle, O., Cross, R.W., Abelson, D.M., Moyer, C.L., Mishra, A.K., Aguilan, J.T., et al. (2021). Protective neutralizing antibodies from human survivors of

Crimean-Congo hemorrhagic fever. Cell *184*, 3486–3501.e21. https://doi.org/10.1016/j.cell.2021.05.001.

Foulongne, V., Guyon, G., Rodière, M., and Segondy, M. (2006). Human Metapneumovirus infection in young children hospitalized with respiratory tract disease. Pediatr. Infect. Dis. J. *25*, 354–359. https://doi.org/10.1097/01.inf.0000207480.55201.f6.

Frank, S., Kammerer, R.A., Mechling, D., Schulthess, T., Landwehr, R., Bann, J., Guo, Y., Lustig, A., Bächinger, H.P., and Engel, J. (2001). Stabilization of short collagen-like triple helices by protein engineering. J. Mol. Biol. *308*, 1081–1089. https://doi.org/10.1006/jmbi.2001.4644.

Gietz, R.D., and Woods, R.A. (2002). Transformation of yeast by lithium acetate/single-stranded carrier DNA/polyethylene glycol method. Methods Enzymol. *350*, 87–96. https://doi.org/10.1016/s0076-6879(02)50957-5.

Gilman, M.S., Castellanos, C.A., Chen, M., Ngwuta, J.O., Goodwin, E., Moin, S.M., Mas, V., Melero, J.A., Wright, P.F., Graham, B.S., et al. (2016). Rapid profiling of RSV antibody repertoires from the memory B cells of naturally infected adult donors. Sci. Immunol. *1*. https://doi.org/10.1126/sciimmunol.aaj1879.

Graham, B.S. (2017). Vaccine development for respiratory syncytial virus. Curr. Opin. Virol. *23*, 107–112. https://doi.org/10.1016/j.coviro.2017.03.012.

Grant, T., Rohou, A., and Grigorieff, N. (2018). cisTEM, user-friendly software for single-particle image processing. eLife *7*, e35383. https://doi.org/10.7554/eLife.35383.

Haas, L.E., Thijsen, S.F., van Elden, L., and Heemstra, K.A. (2013). Human Metapneumovirus in adults. Viruses *5*, 87–110. https://doi.org/10.3390/v5010087.

Hammitt, L.L., Dagan, R., Yuan, Y., Baca Cots, M., Bosheva, M., Madhi, S.A., Muller, W.J., Zar, H.J., Brooks, D., Grenham, A., et al. (2022). Nirsevimab for prevention of RSV in healthy late-preterm and term infants. N. Engl. J. Med. *386*, 837–846. https://doi.org/10.1056/NEJMoa2110275.

Henry, C., Zheng, N.Y., Huang, M., Cabanov, A., Rojas, K.T., Kaur, K., Andrews, S.F., Palm, A.E., Chen, Y.Q., Li, Y., et al. (2019). Influenza virus vaccination elicits poorly adapted B cell responses in elderly individuals. Cell Host Microbe *25*, 357–366.e6. https://doi.org/10.1016/j.chom.2019.01.002.

Hiatt, A., Bohorova, N., Bohorov, O., Goodman, C., Kim, D., Pauly, M.H., Velasco, J., Whaley, K.J., Piedra, P.A., Gilbert, B.E., et al. (2014). Glycan variants of a respiratory syncytial virus antibody with enhanced effector function and in vivo efficacy. Proc. Natl. Acad. Sci. USA *111*, 5992–5997. https://doi.org/10.1073/pnas.1402458111.

Hsieh, C.L., Rush, S.A., Palomo, C., Chou, C.W., Pickens, W., Más, V., and McLellan, J.S. (2022). Structure-based design of prefusion-stabilized human Metapneumovirus fusion proteins. Nat. Commun. *13*, 1299. https://doi.org/10.1038/s41467-022-28931-3.

Huang, J., Chopra, P., Liu, L., Nagy, T., Murray, J., Tripp, R.A., Boons, G.J., and Mousa, J.J. (2021). Structure, immunogenicity, and conformation-dependent receptor binding of the postfusion human Metapneumovirus F protein. J. Virol. *95*, e0059321. https://doi.org/10.1128/JVI.00593-21.

Huang, J., Diaz, D., and Mousa, J.J. (2019). Antibody epitopes of Pneumovirus fusion proteins. Front. Immunol. *10*, 2778. https://doi.org/10.3389/fimmu.2019.02778.

Huang, J., Diaz, D., and Mousa, J.J. (2020). Antibody recognition of the Pneumovirus fusion protein trimer interface. PLoS Pathog. *16*, e1008942. https://doi.org/10.1371/journal.ppat.1008942.

Ionov, S., and Lee, J. (2022). An immunoproteomic survey of the antibody landscape: insights and opportunities revealed by serological repertoire profiling. Front. Immunol. *13*, 832533. https://doi.org/10.3389/fimmu.2022.832533.

Jones, H.G., Battles, M.B., Lin, C.C., Bianchi, S., Corti, D., and McLellan, J.S. (2019). Alternative conformations of a major antigenic site on RSV F. PLoS Pathog. *15*, e1007944. https://doi.org/10.1371/journal.ppat.1007944.

Magro, M., Mas, V., Chappell, K., Vázquez, M., Cano, O., Luque, D., Terrón, M.C., Melero, J.A., and Palomo, C. (2012). Neutralizing antibodies against the preactive form of respiratory syncytial virus fusion protein offer unique possibilities for clinical intervention. Proc. Natl. Acad. Sci. USA *109*, 3089–3094. https://doi.org/10.1073/pnas.1115941109.

Mas, V., Nair, H., Campbell, H., Melero, J.A., and Williams, T.C. (2018). Antigenic and sequence variability of the human respiratory syncytial virus F glycoprotein compared to related viruses in a comprehensive dataset. Vaccine *36*, 6660–6673. https://doi.org/10.1016/j.vaccine.2018.09.056.

Más, V., Rodriguez, L., Olmedillas, E., Cano, O., Palomo, C., Terrón, M.C., Luque, D., Melero, J.A., and McLellan, J.S. (2016). Engineering, structure and immunogenicity of the human Metapneumovirus F protein in the postfusion conformation. PLoS Pathog. *12*, e1005859. https://doi.org/10.1371/journal.ppat.1005859.

McLellan, J.S., Chen, M., Chang, J.S., Yang, Y., Kim, A., Graham, B.S., and Kwong, P.D. (2010). Structure of a major antigenic site on the respiratory syncytial virus fusion glycoprotein in complex with neutralizing antibody 101F. J. Virol. *84*, 12236–12244. https://doi.org/10.1128/JVI.01579-10.

McLellan, J.S., Chen, M., Joyce, M.G., Sastry, M., Stewart-Jones, G.B., Yang, Y., Zhang, B., Chen, L., Srivatsan, S., Zheng, A., et al. (2013a). Structure-based design of a fusion glycoprotein vaccine for respiratory syncytial virus. Science *342*, 592–598. https://doi.org/10.1126/science.1243283.

McLellan, J.S., Chen, M., Leung, S., Graepel, K.W., Du, X., Yang, Y., Zhou, T., Baxa, U., Yasuda, E., Beaumont, T., et al. (2013b). Structure of RSV fusion glycoprotein trimer bound to a prefusion-specific neutralizing antibody. Science *340*, 1113–1117. https://doi.org/10.1126/science.1234914.

Mirdita, M.S.,K., Moriwaki, Y., Heo, L., Ovchinnikov, S., and Steinegger, M. (2022). ColabFold – Making protein folding accessible to all. Preprint at bioRxiv. https://doi.org/10.1101/2021.08.15.456425.

Mousa, J.J., Binshtein, E., Human, S., Fong, R.H., Alvarado, G., Doranz, B.J., Moore, M.L., Ohi, M.D., and Crowe, J.E., Jr. (2018). Human antibody recognition of antigenic site IV on Pneumovirus fusion proteins. PLoS Pathog. *14*, e1006837. https://doi.org/10.1371/journal.ppat.1006837.

Nao, N., Saikusa, M., Sato, K., Sekizuka, T., Usuku, S., Tanaka, N., Nishimura, H., and Takeda, M. (2020). Recent molecular evolution of human Metapneumovirus (HMPV): subdivision of HMPV A2b strains. Microorganisms *8*, 1280. https://doi.org/10.3390/microorganisms8091280.

Ngwuta, J.O., Chen, M., Modjarrad, K., Joyce, M.G., Kanekiyo, M., Kumar, A., Yassine, H.M., Moin, S.M., Killikelly, A.M., Chuang, G.Y., et al. (2015). Prefusion F-specific antibodies determine the magnitude of RSV neutralizing activity in human sera. Sci. Transl. Med. *7*, 309ra162. https://doi.org/10.1126/scitranslmed.aac4241.

Panda, S., Mohakud, N.K., Pena, L., and Kumar, S. (2014). Human Metapneumovirus: review of an important respiratory pathogen. Int. J. Infect. Dis. *25*, 45–52. https://doi.org/10.1016/j.ijid.2014.03.1394.

The IMpact-RSV Study Group (1998). Palivizumab, a humanized respiratory syncytial virus monoclonal antibody, reduces hospitalization from respiratory syncytial virus infection in high-risk infants. Pediatrics *102*, 531–537.

Pettersen, E.F., Goddard, T.D., Huang, C.C., Meng, E.C., Couch, G.S., Croll, T.I., Morris, J.H., and Ferrin, T.E. (2021). UCSF ChimeraX: structure visualization for researchers, educators, and developers. Protein Sci. *30*, 70–82. https://doi.org/10.1002/pro.3943.

Pilaev, M., Shen, Y., Carbonneau, J., Venable, M.C., Rhéaume, C., Lavigne, S., Couture, C., Guarné, A., Hamelin, M.È., and Boivin, G. (2020). Evaluation of pre- and post-fusion Human Metapneumovirus F proteins as subunit vaccine candidates in mice. Vaccine *38*, 2122–2127. https://doi.org/10.1016/j.vaccine.2020.01.047.

Piyaratna, R., Tollefson, S.J., and Williams, J.V. (2011). Genomic analysis of four human Metapneumovirus prototypes. Virus Res. *160*, 200–205. https://doi.org/10.1016/j.virusres.2011.06.014.

Punjani, A., Rubinstein, J.L., Fleet, D.J., and Brubaker, M.A. (2017). cryoSPARC: algorithms for rapid unsupervised cryo-EM structure determination. Nat. Methods *14*, 290–296. https://doi.org/10.1038/nmeth.4169.

Rappazzo, C.G., Tse, L.V., Kaku, C.I., Wrapp, D., Sakharkar, M., Huang, D., Deveau, L.M., Yockachonis, T.J., Herbert, A.S., Battles, M.B., et al. (2021). Broad and potent activity against SARS-like viruses by an engineered human

monoclonal antibody. Science *371*, 823–829. https://doi.org/10.1126/science.abf4830.

Rogers, T.F., Zhao, F., Huang, D., Beutler, N., Burns, A., He, W.T., Limbo, O., Smith, C., Song, G., Woehl, J., et al. (2020). Isolation of potent SARS-CoV-2 neutralizing antibodies and protection from disease in a small animal model. Science *369*, 956–963. https://doi.org/10.1126/science.abc7520.

Ruckwardt, T.J., Morabito, K.M., Phung, E., Crank, M.C., Costner, P.J., Holman, L.A., Chang, L.A., Hickman, S.P., Berkowitz, N.M., Gordon, I.J., et al. (2021). Safety, tolerability, and immunogenicity of the respiratory syncytial virus prefusion F subunit vaccine DS-Cav1: a phase 1, randomised, open-label, dose-escalation clinical trial. Lancet Respir. Med. *9*, 1111–1120. https://doi.org/10.1016/S2213-2600(21)00098-9.

Sadoff, J., De Paepe, E., Haazen, W., Omoruyi, E., Bastian, A.R., Comeaux, C., Heijnen, E., Strout, C., Schuitemaker, H., and Callendret, B. (2021). Safety and immunogenicity of the Ad26.RSV.preF investigational vaccine coadministered With an influenza vaccine in older adults. J. Infect. Dis. *223*, 699–708. https://doi.org/10.1093/infdis/jiaa409.

Sakharkar, M., Rappazzo, C.G., Wieland-Alter, W.F., Hsieh, C.L., Wrapp, D., Esterman, E.S., Kaku, C.I., Wec, A.Z., Geoghegan, J.C., McLellan, J.S., et al. (2021). Prolonged evolution of the human B cell response to SARS-CoV-2 infection. Sci. Immunol. *6*, eabg6916. https://doi.org/10.1126/sciimmunol.abg6916.

Sanchez-Garcia, R., Gomez-Blanco, J., Cuervo, A., Carazo, J.M., Sorzano, C.O.S., and Vargas, J. (2021). DeepEMhancer: a deep learning solution for cryo-EM volume post-processing. Commun. Biol. *4*, 874. https://doi.org/10.1038/s42003-021-02399-1.

Saphire, E.O., Schendel, S.L., Gunn, B.M., Milligan, J.C., and Alter, G. (2018). Antibody-mediated protection against Ebola virus. Nat. Immunol. *19*, 1169–1178. https://doi.org/10.1038/s41590-018-0233-9.

Schuster, J.E., Cox, R.G., Hastings, A.K., Boyd, K.L., Wadia, J., Chen, Z., Burton, D.R., Williamson, R.A., and Williams, J.V. (2015). A broadly neutralizing human monoclonal antibody exhibits in vivo efficacy against both human Metapneumovirus and respiratory syncytial virus. J. Infect. Dis. *211*, 216–225. https://doi.org/10.1093/infdis/jiu307.

Shafagati, N., and Williams, J. (2018). Human Metapneumovirus - what we know now. F1000Res *7*, 135. https://doi.org/10.12688/f1000research.12625.1.

Shirogane, Y., Takeda, M., Iwasaki, M., Ishiguro, N., Takeuchi, H., Nakatsu, Y., Tahara, M., Kikuta, H., and Yanagi, Y. (2008). Efficient multiplication of human Metapneumovirus in Vero cells expressing the transmembrane serine protease TMPRSS2. J. Virol. *82*, 8942–8946. https://doi.org/10.1128/JVI.00676-08.

Skiadopoulos, M.H., Biacchesi, S., Buchholz, U.J., Amaro-Carambot, E., Surman, S.R., Collins, P.L., and Murphy, B.R. (2006). Individual contributions of the human Metapneumovirus F, G, and SH surface glycoproteins to the induction of neutralizing antibodies and protective immunity. Virology *345*, 492–501. https://doi.org/10.1016/j.virol.2005.10.016.

Sok, D., and Burton, D.R. (2018). Recent progress in broadly neutralizing antibodies to HIV. Nat. Immunol. *19*, 1179–1188. https://doi.org/10.1038/s41590-018-0235-7.

Stewart-Jones, G.B.E., Gorman, J., Ou, L., Zhang, B., Joyce, M.G., Yang, L., Cheng, C., Chuang, G.Y., Foulds, K.E., Kong, W.P., et al. (2021). Interprotomer disulfide-stabilized variants of the human Metapneumovirus fusion glycoprotein induce high titer-neutralizing responses. Proc. Natl. Acad. Sci. USA *118*. e2106196118. https://doi.org/10.1073/pnas.2106196118.

Ulbrandt, N.D., Ji, H., Patel, N.K., Barnes, A.S., Wilson, S., Kiener, P.A., Suzich, J., and McCarthy, M.P. (2008). Identification of antibody neutralization epitopes on the fusion protein of human Metapneumovirus. J. Gen. Virol. *89*, 3113–3118. https://doi.org/10.1099/vir.0.2008/005199-0.

van den Hoogen, B.G., Bestebroer, T.M., Osterhaus, A.D., and Fouchier, R.A. (2002). Analysis of the genomic sequence of a human Metapneumovirus. Virology *295*, 119–132. https://doi.org/10.1006/viro.2001.1355.

van den Hoogen, B.G., de Jong, J.C., Groen, J., Kuiken, T., de Groot, R., Fouchier, R.A., and Osterhaus, A.D. (2001). A newly discovered human Pneumovirus isolated from young children with respiratory tract disease. Nat. Med. *7*, 719–724. https://doi.org/10.1038/89098.

van den Hoogen, B.G., Herfst, S., Sprong, L., Cane, P.A., Forleo-Neto, E., de Swart, R.L., Osterhaus, A.D., and Fouchier, R.A. (2004a). Antigenic and genetic variability of human metapneumoviruses. Emerg. Infect. Dis. *10*, 658–666. https://doi.org/10.3201/eid1004.030393.

van den Hoogen, B.G., Osterhaus, D.M., and Fouchier, R.A. (2004b). Clinical impact and diagnosis of human Metapneumovirus infection. Pediatr. Infect. Dis. J. *23*, S25–S32. https://doi.org/10.1097/01.inf.0000108190.09824.e8.

van Erp, E.A., Luytjes, W., Ferwerda, G., and van Kasteren, P.B. (2019). Fc-mediated antibody effector functions During respiratory syncytial virus infection and disease. Front. Immunol. *10*, 548. https://doi.org/10.3389/fimmu.2019.00548.

Vander Heiden, J.A., Stathopoulos, P., Zhou, J.Q., Chen, L., Gilbert, T.J., Bolen, C.R., Barohn, R.J., Dimachkie, M.M., Ciafaloni, E., Broering, T.J., et al. (2017). Dysregulation of B cell repertoire formation in myasthenia gravis patients revealed through deep sequencing. J. Immunol. *198*, 1460–1473. https://doi.org/10.4049/jimmunol.1601415.

Walsh, S.R., and Seaman, M.S. (2021). Broadly neutralizing antibodies for HIV-1 prevention. Front. Immunol. *12*, 712122. https://doi.org/10.3389/fimmu.2021.712122.

Wen, X., Krause, J.C., Leser, G.P., Cox, R.G., Lamb, R.A., Williams, J.V., Crowe, J.E., Jr., and Jardetzky, T.S. (2012). Structure of the human Metapneumovirus fusion protein with neutralizing antibody identifies a Pneumovirus antigenic site. Nat. Struct. Mol. Biol. *19*, 461–463. https://doi.org/10.1038/nsmb.2250.

Wen, X., Mousa, J.J., Bates, J.T., Lamb, R.A., Crowe, J.E., Jr., and Jardetzky, T.S. (2017). Structural basis for antibody cross-neutralization of respiratory syncytial virus and human Metapneumovirus. Nat. Microbiol. *2*, 16272. https://doi.org/10.1038/nmicrobiol.2016.272.

White, J.M., Delos, S.E., Brecher, M., and Schornberg, K. (2008). Structures and mechanisms of viral membrane fusion proteins: multiple variations on a common theme. Crit. Rev. Biochem. Mol. Biol. *43*, 189–219. https://doi.org/10.1080/10409230802058320.

Widmer, K., Zhu, Y., Williams, J.V., Griffin, M.R., Edwards, K.M., and Talbot, H.K. (2012). Rates of hospitalizations for respiratory syncytial virus, human Metapneumovirus, and influenza virus in older adults. J. Infect. Dis. *206*, 56–62. https://doi.org/10.1093/infdis/jis309.

Williams, J.V., Tollefson, S.J., Johnson, J.E., and Crowe, J.E., Jr. (2005). The cotton rat (Sigmodon hispidus) is a permissive small animal model of human Metapneumovirus infection, pathogenesis, and protective immunity. J. Virol. *79*, 10944–10951. https://doi.org/10.1128/JVI.79.17.10944-10951.2005.

Wrammert, J., Smith, K., Miller, J., Langley, W.A., Kokko, K., Larsen, C., Zheng, N.Y., Mays, I., Garman, L., Helms, C., et al. (2008). Rapid cloning of high-affinity human monoclonal antibodies against influenza virus. Nature *453*, 667–671. https://doi.org/10.1038/nature06890.

Xu, J., Zhang, Y., and Williams, J.V. (2018). Development and optimization of a direct plaque assay for trypsin-dependent human Metapneumovirus strains. J. Virol. Methods *259*, 1–9. https://doi.org/10.1016/j.jviromet.2018.05.012.

Yang, C.F., Wang, C.K., Tollefson, S.J., Piyaratna, R., Lintao, L.D., Chu, M., Liem, A., Mark, M., Spaete, R.R., Crowe, J.E., Jr., and Williams, J.V. (2009). Genetic diversity and evolution of human Metapneumovirus fusion protein over twenty years. Virol. J. *6*, 138. https://doi.org/10.1186/1743-422X-6-138.

Zhu, Q., McLellan, J.S., Kallewaard, N.L., Ulbrandt, N.D., Palaszynski, S., Zhang, J., Moldt, B., Khan, A., Svabek, C., McAuliffe, J.M., et al. (2017). A highly potent extended half-life antibody as a potential RSV vaccine surrogate for all infants. Sci. Transl. Med. *9*. https://doi.org/10.1126/scitranslmed.aaj1928.

Zohar, T., Hsiao, J.C., Mehta, N., Das, J., Devadhasan, A., Karpinski, W., Callahan, C., Citron, M.P., DiStefano, D.J., Touch, S., et al. (2022). Upper and lower respiratory tract correlates of protection against respiratory syncytial virus following vaccination of nonhuman primates. Cell Host Microbe *30*, 41–52.e5. https://doi.org/10.1016/j.chom.2021.11.006.

STAR★METHODS

KEY RESOURCES TABLE

REAGENT or RESOURCE	SOURCE	IDENTIFIER
Antibodies		
Goat polyclonal anti-human IgG Fc conjugated to horseradish peroxidase	Thermo Fisher Scientific	Cat#31413, RRID: AB_429693
Mouse monoclonal anti-human CD19	BioLegend	Cat#302216, RRID: AB_314246
Mouse monoclonal anti-human CD3	BioLegend	Cat#300430, RRID: AB_893299
Mouse monoclonal anti-human CD8	BioLegend	Cat#344710, RRID: AB_2044010
Mouse monoclonal anti-human CD14	Invitrogen	Cat#45-0149-42, RRID: AB_1518736
Mouse monoclonal anti-human CD16	BioLegend	Cat#360712, RRID: AB_2562955
Mouse monoclonal anti-human IgM	BD Biosciences	Cat#747877, RRID: AB_2872339
Mouse monoclonal anti-human IgD	BioLegend	Cat#348218, RRID: AB_11203722
Goat polyclonal anti-human IgA	Abcam	Cat#Ab98553, RRID: AB_10672542
Mouse monoclonal anti-human IgG	BD Biosciences	Cat#563246, RRID: AB_2738092
Mouse monoclonal anti-human CD27	BD Biosciences	Cat#740167, RRID: AB_2739920
Goat polyclonal F(ab')2 anti-human kappa FITC	SouthernBiotech	Cat#2062-02, RRID: AB_2795737
Goat polyclonal F(ab')2 anti-human lambda FITC	SouthernBiotech	Cat#2072-02, RRID: AB_2795767
Mouse monoclonal anti-hMPV N protein	Millipore	Cat# MAB80138, RRID: AB_11211020
Rabbit polyclonal anti-mouse IgG conjugated to horseradish peroxidase	Millipore	Cat# AP160P, RRID: AB_92531
Monoclonal anti-hMPV F protein antibodies MF14, MF1 and MF16	Battles et al., 2017	N/A
Sheep anti-mouse IgG conjugated to horseradish peroxidase	Cytiva	Cat#RPN4201, RRID: N/A
Bacterial and virus strains		
hMPV isolate A2 TN/94/49	Piyaratna et al., 2011	N/A
GFP-expressing hMPV recombinant virus derived from isolate A1 NL/1/00	de Graaf et al., 2007	N/A
GFP-expressing hMPV recombinant virus derived from isolate B1 NL/1/99	de Graaf et al., 2007	N/A
hMPV isolate B2 NL/1/94	van den Hoogen et al., 2004a	N/A
hMPV isolate A2 SP/2/18	This paper	N/A
hMPV isolate B1 SP/1/15	This paper	N/A
Biological samples		
Healthy human peripheral blood mononuclear cells and sera samples	Dartmouth Hitchcock Medical Center	N/A
Cotton rat sera samples	Sigmovir Biosystems, Inc.	N/A
Chemicals, peptides, and recombinant proteins		
Prefusion-stabilized hMPV F A1	Battles et al., 2017	N/A
Prefusion-stabilized hMPV F B2	Bar-Peled, et al., 2019	N/A
Prefusion-stabilized RSV F A1 DS-Cav1	McLellan et al., 2013a	N/A
Postfusion hMPV F A1	Mas et al., 2018	N/A
Prefusion-stabilized hMPV F A1 DS-CavEs2 (NL/1/00)	Hsieh et al., 2022	N/A
Pluronic F-68	Gibco	Cat#24040032
StrepTactin Sepharose resin	IBA	Cat#2-1201
Superose 6 Increase 10/300 column	GE Healthcare	Cat#GE29-0915-96

(*Continued on next page*)

Continued

REAGENT or RESOURCE	SOURCE	IDENTIFIER
Superdex 200 Increase 10/300 column	GE Healthcare	Cat#GE28-9909-44
1-Step Ultra TMB-ELISA Substrate Solution	Thermo Fisher Scientific	Cat#34029
Propidium Iodide	Sigma	Cat#P4170-25MG
NP-40	Thermo Fisher Scientific	Cat#85124
RNaseOUT	Invitrogen	Cat#10777019
Dithiothreitol	Thermo Fisher Scientific	Cat#R0861
Polyethylene glycol 3350	Sigma	Cat#202444
Salmon Sperm DNA solution	Invitrogen	Cat#15632011
Lithium Acetate	Sigma	Cat#517992
KappaSelect resin	Cytiva	Cat#17545803
LambdaFabSelect resin	Cytiva	Cat#17548203
Strep-Tactin APC	IBA Lifesciences	Cat#6-5010-001
OptiMEM	Gibco	Cat#31985-070
Trypsin	Corning	Cat#25-052-CI
Triton X-100	Sigma	Cat#T8787
Bovine Serum Albumin (BSA)	Sigma	Cat#A9418
AEC (3-Amino-9-ethylcarbazole) chromogen detection solution	Sigma	Cat#AEC101
Iscove's Modified Dulbecco's Medium	Gibco	Cat#12440053
Fetal Bovine Serum	Gibco	Cat#10082147
Trypsin, TPCK-treated	Sigma	Cat#4352157
Dulbecco's Modified Eagle Medium	Gibco	Cat#11965084
OPD (*o*-Phenylenediamine dihydrochloride) peroxidase substrate	Sigma	Cat#P9187
Hank's balanced salt solution	Lonza	Cat#10-527F
Critical commercial assays		
EasySep Direct Human B Cell Isolation Kit	Stem Cell Technologies	Cat#19674
SuperScript IV Reverse Transcriptase	Thermo Fisher Scientific	Cat#18090050
HotStarTaq Plus DNA Polymerase Kit	Qiagen	Cat#203646
RNeasy Purification Kits	Qiagen	Cat#74106
SuperScript II Reverse Transcriptase	Invitrogen	Cat#18064-022
iQ SYBR Green Supermix	Bio-Rad	Cat#1708880
Deposited data		
hMPV F – ADI-61026 – MPE8 structure	This paper	PDB: 8CW9
hMPV F – MPV458 structure	Huang et al., 2020	PDB: 6W16
RSV F – D25 structure	McLellan et al., 2013b	PDB: 4JHW
RSV F – AM22 structure	Jones et al., 2019	PDB: 6DC5
Experimental models: Cell lines		
Human: FreeStyle 293F Cells	Thermo Fisher Scientific	Cat#R79007
Hamster: Chinese Hamster Ovary Cells	DSMZ	Cat#ACC110
Rhesus Monkey: LLC-MK2 Cells	ATCC	Cat#CCL-7
African Green Monkey: Vero-118 Cells	van den Hoogen et al., 2004b	N/A
Human: Caco-2 Cells	ATCC	Cat#HTB-37
Experimental models: Organisms/strains		
S. cerevisiae	Adimab, LLC	N/A
S. hispidus	Sigmovir Biosystems, Inc.	N/A

(*Continued on next page*)

Continued

REAGENT or RESOURCE	SOURCE	IDENTIFIER
Oligonucleotides		
Primers used for RT-PCR and nested PCRs	Sakharkar et al., 2021	N/A
Oligo (dT) Primer	Invitrogen	Cat#AM5730G
Primers specific to β-actin (TACGCCAACACAGTGCTGTCT and TCTGCATCCTGTCGGCAAT)	This paper	N/A
Primers specific to hMPV L polymerase (AGGGGTTCGGAATCCTGATAGG and GTTTCACAGTCCTTCTCATTTGGG)	This paper	N/A
Software and algorithms		
FlowJo	FlowJo	www.flowjo.com
GraphPad Prism 9	GraphPad	https://www.graphpad.com/scientific-software/prism/
ForteBio Data Analysis Software, version 11.1	Sartorius	https://www.sartorius.com/en/products/protein-analysis/octet-bli-detection/octet-systems-software
cryoSPARC v3.2.0	Punjani et al., 2017	https://cryosparc.com/
DeepEMhancer	Sanchez-Garcia et al., 2021	https://github.com/rsanchezgarc/deepEMhancer
SabPred server	Dunbar et al., 2016	http://opig.stats.ox.ac.uk/webapps/newsabdab/sabpred/
UCSF ChimeraX	Pettersen et al., 2021	https://www.cgl.ucsf.edu/chimerax/
Coot	Casanal et al., 2020	https://www2.mrc-lmb.cam.ac.uk/personal/pemsley/coot/
Phenix	Adams et al., 2010	http://www.phenix-online.org/
ISOLDE	Croll, 2018	https://isolde.cimr.cam.ac.uk/download/
ColabFold	Evans et al., 2022; Mirdita et al., 2022	https://github.com/sokrypton/ColabFold
cisTEM	Grant et al., 2018	https://cistem.org/
Other		
Anti-human IgG Fc Capture (AHC) biosensors	Sartorius	Cat#18-5060
Streptavidin (SA) biosensors	Sartorius	Cat#18-5019

RESOURCE AVAILABILITY

Lead contact

Further information and requests for resources and reagents should be directed to and will be fulfilled by the lead contact, Laura M. Walker (lwalker@adagiotx.com).

Materials availability

IgGs are available under MTA from Adimab, LLC.

Data and code availability

The hMPV F – ADI-61026 – MPE8 structure has been deposited to the Protein Data Bank and is publicly available as of the date of publication. This paper also analyzes existing, publicly available structure data. Accession numbers are listed in the key resources table. All other data are available in the manuscript or supplemental information. This paper does not report original code. Any additional information required to reanalyze the data reported in this paper is available from the lead contact upon request.

EXPERIMENTAL MODEL AND SUBJECT DETAILS

Human subjects

A total of 16 healthy donors were recruited for this study (Table S1). Eight donors were between the ages of 21 and 27 (young adult cohort) and eight donors were over the age of 65 (elderly cohort). All donors were screened for seropositivity to hMPV and RSV to confirm prior exposure to each virus. Only one donor, IML2992 had a known clinical history of hospitalization due to

hMPV-associated disease. All volunteers gave informed consent using a template approved by the Dartmouth-Hitchcock Hospital (D-HH) Human Research Protection Program (Institutional Review Board) with the clinical component coordinated by the Clinical Research Unit of D-HH. This study was unblinded and not randomized.

Animal studies

Male *Sigmodon hispidus* cotton rats between 6 and 8 weeks of age (Source: Sigmovir Biosystems, Inc., Rockville MD) were maintained and handled under veterinary supervision in accordance with National Institutes of Health guidelines and Sigmovir IACUC approved animal study protocol. The cotton rats were group housed and provided with standard rodent chow (Harlan, #7004) and tap water *ad libitum*. Cotton rats were randomly divided into 4 groups of 5 animals for challenge studies.

Cell lines

Vero subclone 118 (Vero-118) (van den Hoogen et al., 2004b) cells, derived from a female green monkey (*Chlorocebus sabaeus*), were grown in Iscove's modified Dulbecco's medium (IMDM; Gibco, catalog no. 12440053) supplemented with 10% fetal calf serum (FCS) (Gibco, catalog no. 10082147) and glutamine (4 mM). Caco-2 cells, derived from a 72-year-old male with colorectal adenocarcinoma, were grown in Dulbecco's Modified Eagle medium (DMEM; Gibco, catalog no. 11965084) supplemented with 20% FCS. LLC-MK2 cells, derived from rhesus monkeys (*Macaca mulatta*) of unknown sex, were grown in OptiMEM supplemented with 10% FCS. Chinese Hamster Ovary (CHO) cells, derived from female Chinese hamsters (*Cricetulus griseus*), were grown in CHOgro expression media (Mirus, catalog no. MIR 6200).

METHOD DETAILS

hMPV and RSV antigens

Prefusion-stabilized hMPV F (preF) A1 (NL/1/00) (Battles et al., 2017) and B2 (TN/99/419) (Bar-Peled et al., 2019) include disulfide (A113C/A339C) and proline (A185P) substitutions for prefusion stabilization (Stewart-Jones et al., 2021. Battles et al., 2017). The putative protease site has been mutated from ENPRQSR to the furin cleavage site ENPRRRR. Additionally, G294E from B2 was introduced into the A1 construct and a H368N substitution was incorporated into both constructs. Gibson assembly was used to construct the genes encoding the antigen probes (amino acids 1 – 490) into plasmids containing a C-terminal T4 fibritin trimerization motif (Frank et al., 2001) followed by His and StrepTagII tags. Plasmids encoding the antigen and furin were transiently co-transfected into FreeStyle 293F cells (Thermo Fisher, catalog no. R79007) at a 4:1 ratio using polyethyleneimine (PEI). Three hours post-transfection, 5 μM kifunensine was added, as well as Pluronic F-68 (Gibco, catalog no. 24040032) to a final concentration of 0.1% v/v. Six days post-transfection, supernatant was filtered and buffer exchanged into PBS using tangential flow filtration. Samples were purified by StrepTactin resin (IBA, catalog no. #2-1201) followed by size-exclusion chromatography (SEC) using a Superose 6 Increase 10/300 column (GE Healthcare, catalog no. GE29-0915-96) in 2 mM Tris pH 8.0, 200 mM NaCl, and 0.02% NaN_3 running buffer. The generation of prefusion-stabilized RSV F A1, also known as DS-Cav1 has been previously described (McLellan et al., 2013a) and was similarly expressed and purified without the addition of Pluronic F-68.

Postfusion hMPV F (postF) A1 was constructed as previously described (Más et al., 2016) with removal of fusion peptide residues and modification of the cleavage site to ENPRQSKKRKRR. Transient transfection of FreeStyle 293F cells was as described above. After six days, the medium was harvested and buffer exchanged into 20 mM Tris, pH 8.0, 20 mM imidazole pH 8.0, 300 mM NaCl and passed over Ni-NTA resin. After wash steps, protein was eluted from resin with 20 mM Tris, pH 8.0, 250 mM imidazole pH 8.0, 300 mM NaCl. The sample was then concentrated and passed over a Superose 6 Increase 10/300 column with 2 mM Tris pH 8.0, 200 mM NaCl, and 0.02% NaN3 running buffer. After purification, protein was heated at 70 °C for 10 min to trigger any residual prefusion to postfusion F.

For structural studies, prefusion F construct DS-CavEs2 (strain NL/1/00; substitutions: G294E/A185P/A140C-A147C/L110C-N322C/T127C-N153C/T365C-V463C/L219K/V231I/E453Q/ENPRRRR cleavage site) (Hsieh et al., 2022) was expressed and purified as described above for the hMPV prefusion F antigens. A monomeric construct of DS-CavEs2 was generated by removing the T4 fibritin trimerization motif and introducing a second StrepTagII. Monomeric DS-CavEs2 was purified using Ni-NTA resin followed by SEC with a Superdex 200 Increase 10/300 column (GE Healthcare, catalog no. #GE28-9909-44).

Enzyme-linked immunosorbent assays

For hMPV serum binding studies, 96-well high-binding polystyrene ELISA plates (Corning, catalog no. 3690) were coated with 25 μl per well of hMPV F antigens diluted to 5 μg/ml in PBS (pH 7.4) and incubated overnight at 4 °C. Wells were washed three times with PBS and then blocked with 5% (w/v) nonfat dried milk (NFDM) in PBS for 1 h at 37 °C. After removal of the blocking solution, serial dilutions of human serum in 5% NFDM-PBS were added to the wells and allowed to incubate for 1 h at 37 °C. Plates were washed three times with PBS, and then secondary cross-adsorbed anti-human IgG–horseradish peroxidase (HRP) (Thermo Fisher Scientific, catalog no. 31413) detection antibody was added at 1:8000 dilution in 5% NFDM-PBS and incubated for 1 h at 37 °C. After washing three times with PBS, 25 μl per well of 1-Step Ultra TMB-ELISA Substrate Solution (Thermo Fisher Scientific, catalog no. 34029) was added to detect binding, followed by addition of an equal volume of stop reagent. Absorbance was measured at 450 nm using a SpectraMax microplate reader M3 (Molecular Devices).

Memory B cell staining and single B cell sorting

B cells were purified directly from human peripheral blood samples using the EasySep Direct Human B Cell Isolation Kit (Stem Cell Technologies catalog no. 19674). Purified B cells were stained using anti-human CD19 [phycoerythrin (PE)–Cy7; BioLegend, catalog no. 302216), CD3 (peridinin-chlorophyll-protein, PerCP-Cy5.5; BioLegend, catalog no. 300430), CD8 (PerCP-Cy5.5; BioLegend, catalog no. 344710), CD14 (PerCP-Cy5.5; Invitrogen, catalog no. 45-0149-42), CD16 (PerCP-Cy5.5; BioLegend, catalog no. 360712), IgM (BV711; BD Biosciences, catalog no. 747877), IgD (allophycocyanin (APC)–Cy7; BioLegend, catalog no. 348218), IgA (AlexaFluor, Abcam, catalog no. Ab98553), IgG (BV605; BD Biosciences, catalog no.563246), CD27 (BV510; BD Biosciences, catalog no. 740167), propidium iodide (PI) (Sigma-Aldrich, catalog no. P4170), and a freshly prepared hMPV PreF A, hMPV PreF B, or RSV PreF A tetramers.

Class-switched ($CD19^+CD3^-CD8^-CD14^-CD16^-PI^-IgM^-IgD^-$) B cells that showed reactivity with PE- and APC-labeled pools of hMPV preF A and preF B tetramers were single-cell index–sorted using a BD FACSAria II Fusion (BD Biosciences) into 96-well polypropylene microplates (Corning, catalog no. 07-200-95) containing 20 μl per well of lysis buffer [5 μl of 5× first-strand SuperScript IV (SSIV) complementary DNA buffer (Invitrogen, catalog no. 18090050B), 1.25 μl of dithiothreitol (Thermo Fisher Scientific, catalog no. R0861), 0.625 μl of NP-40 (Thermo Fisher Scientific, catalog no. 85124), 0.25 μl of RNaseOUT (Invitrogen, catalog no.10777019), and 12.85 μl of dH_2O]. Plates were immediately spun down at 1000*g* for 30 s and stored at -80 °C until use. Flow cytometry data were analyzed using FlowJo software.

Amplification and cloning of antibody variable genes

Human antibody variable gene transcripts (VH, Vκ, and Vλ) were amplified by RT-PCR using SuperScript IV enzyme (Thermo Fisher Scientific, catalog no. 18090050), followed by nested PCR using cocktails of variable region and IgM-, IgD-, IgA-, and IgG-specific constant-region primers and HotStarTaq Plus DNA Polymerase (Qiagen, catalog no. 203646), as previously described (Sakharkar et al., 2021). The primers used in the second round of nested PCR contained 40 base pairs of 5′ and 3′ homology for linearized yeast expression vectors to allow cloning by homologous recombination. Amplified variable gene transcripts were transformed into in *S. cerevisiae* using the lithium acetate method for chemical transformation (Gietz and Woods, 2002). For each transformation reaction, 1×10^6 yeast cells were mixed and incubated with 240 μl of polyethylene glycol 3350 [50% (w/v)] (Sigma-Aldrich, catalog no. 202444), 36 μl of 1 M lithium acetate (Sigma-Aldrich, catalog no. 517992), 10 μl of denatured salmon sperm DNA (Invitrogen, catalog no. 15632011), 67 μl of sterile water, 200 ng of the digested expression vectors, and 10 μl each of unpurified VH and VL PCR products at 42 °C for 45 min. After transformation, the yeast were washed twice with sterile water, resuspended in selective media, and plated. After a 48 h incubation at 30 °C, individual yeast colonies were picked for Sanger sequencing.

Expression and purification of IgG and Fab

MAbs used for binding experiments, competition assays, and neutralization assays were produced as full-length IgG1 proteins in *S. cerevisiae* cultures, as previously described (Sakharkar et al., 2021). Briefly, yeast cultures were incubated in 24-well plates at 30 °C and 80% relative humidity with shaking at 450 rpm in Multitron shakers (Infors HT). After 6 days of growth, the culture supernatants were harvested by centrifugation, and IgGs were purified by protein A affinity chromatography. IgGs bound to the agarose were eluted with 200 mM acetic acid with 50 mM NaCl (pH 3.5) and neutralized with 1/8 (v/v) 2 M HEPES (pH 8.0).

To generate Fabs for kinetics, competitive binning, and structural studies, IgGs were digested with papain for 2 h at 30 °C, followed by the addition of iodoacetamide to terminate the reaction. The mixtures were passed over protein A agarose to remove Fc fragments and undigested IgG. The flow-through of the protein A resin was passed over either KappaSelect resin (Cytiva, catalog no. 17545803) or LambdaFabSelect resin (Cytiva, catalog no.17548203) for antibodies using the κ or λ light chains, respectively. The Fabs captured on the resin surface were eluted using 200 mM acetic acid with 50 mM NaCl (pH 5.2) and neutralized with 1/8 (v/v) 2 M HEPES (pH 8.0).

For *in vivo* protection studies, mAbs were produced as full-length IgG1 proteins in CHO cells as previously described (Rappazzo et al., 2021). Briefly, the VH- and VL-encoding genes were subcloned into heavy- and light-chain vectors and transiently transfected into CHO cells. After 6 days, the supernatants containing the IgGs were harvested by centrifugation and purified by protein A-affinity chromatography. Bound IgGs were eluted and further purified by size exclusion chromatography (SEC) to at least 95% purity, then buffer-exchanged into 150 mM NaCl with 20 mM histidine, pH 6.0.

BLI kinetic measurements

Apparent IgG binding affinities were measured by BLI using a ForteBio Octet HTX instrument (Sartorius) as previously described (Sakharkar et al., 2021). All reagents were formulated in PBSF [PBS with 0.1% (w/v) Bovine Serum Albumin (BSA)], and all binding steps were performed at an orbital shaking speed of 1000 rpm and 25 °C. To measure IgG binding to recombinant antigens, anti-human IgG Fc Capture (AHC) biosensors (Sartorius, catalog no. 18-5060) were used to capture the IgGs (100 nM, 0.6 to 1.2 nm) and incubated in PBSF for a minimum of 30 min. For experiments involving Strep-tag–encoding antigens, the IgG-loaded biosensors were incubated in a biocytin solution (100 μM) for 10 min to saturate remaining streptavidin binding sites. After a short (60 s) baseline step in PBSF, the IgG-loaded biosensors were exposed (180 s) to the antigen at 100 nM and then dipped (180 s) into PBSF to measure any dissociation of the antigen from the biosensor surface. For binding responses > 0.1 nm, data were aligned, interstep corrected (to the association step), and fitted to a 1:1 binding model using the ForteBio Data Analysis Software, version 11.1.

To measure Fab binding affinities, streptavidin biosensors (Sartorius, catalog no. 18-5019) were used to immobilize biotinylated antigens (100 nM, 1.0 to 2.0 nm) and then incubated in PBSF for a minimum of 30 min. After a short (60 s) baseline step in PBSF, the antigen-loaded biosensors were exposed (180 s) to the Fab at 100 nM and then dipped (180 s) into PBSF to measure any dissociation of the Fabs from the biosensor surface. For binding responses > 0.1 nm, data were aligned, interstep corrected (to the association step), and fitted to a 1:1 binding model using the ForteBio Data Analysis Software, version 11.1.

Competition analysis using BLI

Competition binding of IgGs to RSV preF was evaluated using a ForteBio Octet HTX instrument (Sartorius) as previously described (Sakharkar et al., 2021). All reagents were formulated in PBSF [PBS with 0.1% (w/v) BSA], and all binding steps were performed at an orbital shaking speed of 1000 rpm and 25 °C. Briefly, IgGs (300 nM) were captured onto anti-human IgG (AHC) biosensors (Sartorius, catalog no. 18-5060) to a sensor response of 1.0 to 1.4 nm. An inert IgG (0.5 mg/ml) was used to occupy any remaining binding sites on the biosensor then equilibrated in PBSF for a minimum of 30 min. To assess any cross-interactions between IgG on the sensor surface and the secondary IgG, the loaded and blocked sensors were exposed (90 s) to secondary IgG (300 nM) before the binning analysis. The biosensors were then subjected to a second short (60 s) baseline step in PBSF, followed by an association step (180 s) to RSV preF (200 nM) followed by exposure to a second IgG for competition assessment (300 nM). The data were *y*-axis–normalized, and interstep was corrected using the ForteBio Data Analysis Software version 11.0. Additional binding by the secondary molecule indicates an unoccupied epitope (noncompetitor), whereas the absence of additional binding indicates epitope blocking (competitor).

Competitive binning

Competitive binning experiments were performed by evaluating IgG binding to hMPV F in the presence and absence of pre-complexed competitor Fab, as previously described (Fels et al., 2021). Briefly, hMPV preF A1 (25 nM) was complexed with competitor Fab (0.5 μM) for 30 min on ice. The antigen-Fab complex was then incubated for 5 min with yeast expressing anti-hMPV IgG. After washing with PBSF to remove unbound antigen, the bound antigen was detected using Strep-Tactin APC (IBA Lifesciences, catalog no. 6-5010-001) and antibody light chain was detected using Goat F(ab')2 anti-human kappa FITC (SouthernBiotech, catalog no. 2062-02) and Goat F(ab')2 anti-human lambda FITC (SouthernBiotech, catalog no. 2072-02). The samples were analyzed by flow cytometry using a FACSCanto II (BD Biosciences). For mAbs that displayed detectable binding to hMPV preF A1 in the absence of a competitor Fab, competitive binding was evaluated based on the fold reduction in antigen binding observed in the presence of the competitor Fabs. Fold-reductions greater than 4-fold were classified as competitive binding.

In vitro neutralization assays

The isolation and use of hMPV isolate A2 TN/94/49 has been previously described (Piyaratna et al., 2011; Xu et al., 2018). HMPV A2 virus from isolate TN/94/49 was propogated in LLC-MK2 cells in OptiMEM (Gibco, catalog no. 31985-070) supplemented with 0.1% trypsin (Corning, catalog no. 25-052-CI). Virus was harvested after 7 d and stored at -80 °C until use in sucrose solution, as previously described (Williams et al., 2005). For neutralization experiments, heat inactivated cotton rat sera samples were diluted 1:10 with OptiMEM containing 1% trypsin and serially diluted 1:4, or monoclonal antibodies were diluted 1:10 with OptiMEM containing 1% trypsin to 10 μg/ml and serially diluted 1:10. Diluted sera or mAbs were incubated with 25-50 PFU hMPV A2 (TN/94/49) virus in equal volume for 1 h at room temperature and inoculated in duplicates onto confluent LLC-MK2 cell monolayers in 24 well plates. After 1 h incubation at 37 °C in a 5% CO2 incubator, the wells were overlayed with 0.75% methylcellulose medium. After 7 days of incubation, the overlays were removed, and the cells were fixed for 1 h and air-dried for immuno-staining. Cells were permeabilized with PBS containing 0.4% Triton X-100 (Sigma, catalog no. T8787) for 20 min at room temperature. After blocking wells with 1% BSA (Sigma, catalog no. A9418) in PBS, mouse anti-hMPV N protein (Millipore, catalog no. MAB80138) at a 1:1000 dilution in 1% BSA was added to each well, followed by washes and incubation with HRP conjugated Rabbit anti-mouse IgG (Millipore, catalog no. AP160P) diluted at 1:1000 in 1% BSA. AEC (3-Amino-9-ethylcarbazole) chromogen detection solution (Sigma, catalog no. AEC101) was added to each well and incubated at room temperature for 2 h. Visible plaques were counted and represented as percent of virus control without antibody addition, and values were used to calculate half-maximal plaque-reduction neutralization titers or concentrations ($PRNT_{50}$ or neutralization IC_{50}).

High titer stocks of GFP-expressing hMPV recombinant viruses derived from isolates A1 NL/1/00 and B1 NL/1/99 (de Graaf et al., 2007) and the non-recombinant hMPV B2 isolate NL/1/94. hMPV NL/1/00 were produced in Vero-118 (van den Hoogen et al., 2004b) cells in IMDM (Gibco, catalog no. 12440053) and 4 μg/ml TPCK-trypsin (Sigma, catalog no. 4352157). Viral stocks for hMPV isolates A2 SP/2/18, B1 SP/1/15, and additional test stocks for GFP-recombinant isolate NL/1/99 were produced in Caco-2 cells in DMEM (Gibco, catalog no. 11965084) supplemented with 2% FCS without trypsin. After 5 days, all the cultures were harvested and stored in 25% sucrose at -80 °C. Virus stocks were titrated in Vero-118 cells grown in 96-well plates with infection media: IMDM supplemented with 5% FCS without trypsin. Briefly, confluent monolayers of cells were inoculated with serial dilutions of viral stocks and incubated at 37 °C. After 24 h, wells were washed with PBS then fixed with a solution of methanol 20% and hydrogen peroxide 2%. Infected cells were then detected using a pool of mAbs specific for the hMPV F protein (MF14, MF1 and MF16) (Battles et al., 2017), peroxidase-conjugated anti-mouse secondary antibody (Cytiva, catalog no. RPN4201), and subsequent addition of AEC chromogen (Sigma, catalog no. AEC101). Viral foci forming units (FFU) were counted by microscope and all viral stocks achieved a titer of 10^6-10^7 FFU/ml.

For neutralization experiments, viral stocks (0.03 FFU/cell) were mixed in infection medium for 30 min at room temperature with serial dilutions of heat-inactivated donor sera or monoclonal antibodies before being added to cultures of Vero-118 cells growing in 96-well plates. For GFP-recombinant viruses, media was replaced by PBS 36 h after infection and GFP fluorescence was measured by an Infinite M200 PRO microplate reader (Tecan). For non-recombinant viruses, media was removed 48 h after infection, cells were washed with PBS, and fixed with formaldehyde 4% in PBS. Infected cells were quantified by ELISA using a pool of mAbs specific for the hMPV F protein (MF14, MF1 and MF16) (Battles et al., 2017), peroxidase-conjugated anti-mouse secondary antibody (Cytiva, catalog no. RPN4201) and OPD Peroxidase Substrate (Sigma, catalog no. P9187). Optical densities were read at 492 nm using an Infinite M200 PRO microplate reader (Tecan). For both recombinant and non-recombinant viruses, values were expressed as percent of a virus control without antibody and curves were fit to determine half-maximal neutralization titers or inhibitory concentrations (NT_{50} or neutralization IC_{50}, respectively).

Cotton rat challenge model

20 male cotton rats were divided into 4 groups of 5 animals that were dosed intramuscularly with one of four mAbs at 1.0 mg/kg in 0.2ml (0.1ml per hind leg) 24 h prior to challenge with 10^5 PFU of hMPV A2 (TN/94/49). Serum samples were collected immediately prior to challenge by retro-orbital bleed under isoflurane anesthesia, incubated at room temperature for 4 h, then isolated by centrifugation at 2,000 RPM for 10 min at room temperature. Four days post infection, the animals were sacrificed via CO2 intoxication. The nasal tissue along with the lung *en bloc* were harvested for determining viral load. Serum samples were collected from all animals prior to the treatment, prior to the hMPV/A2 challenge, and prior to termination on day 4. Cotton rat protection studies were not repeated for non-technical replicates.

Viral titration of lung and nose homogenates

Harvested lung and nasal tissues were homogenized in CK28 homogenization tubes (Bertin, catalog no. P000935-LYSK0-A.0) in 10 parts [w/v] homogenization media containing Hank's balanced salt solution (HBSS; Lonza, catalog no. 10-527F) supplemented with 0.218 M Sucrose and 4.4 mM glutamate. Lung and nose homogenates were clarified by centrifugation at 2,000 RPM for 10 min at 2-8 °C and diluted in OptiMEM (Gibco, catalog no. 31985-070) supplemented with 0.1% trypsin (Corning, catalog no. 25-052-CI). Confluent LLC-MK2 monolayers were infected in duplicates with diluted homogenates in 24-well plates. After 1 h incubation at 37°C in a 5% CO_2 incubator, the wells were overlayed with 0.75% methylcellulose medium. After 7 days of incubation, the overlays were removed, and the cells were fixed for 1 h and air-dried for immuno-staining. Cells were permeabilized with PBS containing 0.4% Triton X-100 (Sigma, catalog no. T8787) for 20 min at room temperature. Upon blocking the wells with 1% BSA (Sigma, catalog no. A9418) diluted in PBS, mouse anti-hMPV N protein (Millipore, catalog no. MAB80138) at a 1:1000 dilution in 1% BSA was added to each well, followed by washes and then incubation with HRP-conjugated Rabbit anti-mouse IgG (Millipore, catalog no. AP160P) diluted at 1:1000 in 1% BSA. AEC Chromogen detection solution (Sigma, catalog no. AEC101) was added to each well and incubated at room temperature for 2 h. Visible plaques were counted, and virus titers were quantified as plaque forming units per gram of tissue.

Viral mRNA quantitation

Total RNA was extracted from homogenized lung tissue using RNeasy purification kits (Qiagen, catalog no. 74106). Complementary DNA (cDNA) was prepared from 1 μg total RNA in 20 μl reactions containing SuperScript II Reverse Transcriptase (Invitrogen, catalog no. 18064-022) and 1 μl oligo (dT) primer (Invitrogen, catalog no. AM5730G). For real-time quantitative PCR (qPCR), 25 μl reactions containing iQ SYBR Green Supermix (Bio-Rad, catalog no. 1708880), 3 μl cDNA, and 0.5 mM each of primers specific to either β-actin (TACGCCAACACAGTGCTGTCT and TCTGCATCCTGTCGGCAAT) or hMPV L polymerase (AGGGGTTCGGAATCCTGATAGG and GTTTCACAGTCCTTCTCATTTGGG) were performed in duplicate in 96-well plates (Bio-Rad, catalog no. 2239441). Amplifications were performed in a Bio-Rad iCycler (Bio-Rad, catalog no. 170-8740) for 1 cycle of 95 °C for 3 min, followed by 40 cycles of 95 °C for 10 s, 60 °C for 10 s, and 72 °C for 15 s. The baseline cycles and cycle threshold (Ct) were calculated by the iQ5 software in the PCR Base Line Subtracted Curve Fit mode. Ct values were converted to relative expression units by comparison to standard curves generated by plotting Ct versus $\log_{10}$ dilution factor for serially diluted positive control β-actin or hMPV L cDNA. HMPV L mRNA relative expression values were then normalized to corresponding β-actin mRNA relative expression values for each sample to calculate normalized relative hMPV mRNA copies.

Cryo-EM sample preparation and data collection

Purified DS-CavEs2 (a prefusion-stabilized hMPV F variant) at 0.36 mg/ml was incubated with a 1.5-fold molar excess of ADI-61026 Fab in 2 mM Tris pH 8.0, 200 mM NaCl, and 0.02% NaN_3 at room temperature for 10 min. The sample was mixed with 0.075% A8-35 then immediately deposited on a plasma-cleaned CF-1.2-1.3 grid before being blotted for 4 sec with -2 force in a Vitrobot Mark IV and plunge-frozen into liquid ethane. A total of 3,098 micrographs were collected from a single grid and imaged by a FEI Titan Krios equipped with a K3 direct electron detector (Gatan). Data were collected at a magnification of 29,000x, corresponding to a calibrated pixel size of 0.81 Å/pix. Full data collection parameters are reported in Table S4.

Purified monomeric DS-CavEs2 at 0.2 mg/ml was incubated with a 1.2-fold molar excess of ADI-61026 Fab and a 2-fold molar excess of ADI-61128 in 2 mM Tris pH 8.0, 200 mM NaCl, and 0.02% NaN_3 at room temperature for 10 min. The sample was deposited on a plasma-cleaned CF-1.2-1.3 grid before being blotted for 4 sec with -2 force in a Vitrobot Mark IV (10 °C, 100% humidity) and plunge-frozen into liquid ethane. A total of 837 micrographs were collected from a single grid and imaged by a 200 kV Glacios

equipped with a Falcon 4 direct electron detector (ThermoFisher). Data were collected at a magnification of 150,000x, corresponding to a calibrated pixel size of 0.94 Å/pix. Full data collection parameters are reported in Table S4.

Cryo-EM data processing

HMPV F – ADI-61026 – MPE8 micrographs were imported to cryoSPARC Live v3.2.0 (Punjani et al., 2017) and processed for motion correction, CTF estimation, micrograph curation, particle picking, and particle curation via iterative rounds of 2D classification. The curated particles in corresponding micrographs were further processed in cryoSPARC v3.2 to obtain a final global reconstruction with additional rounds of 2D classification, *ab initio* reconstruction, iterative rounds of heterogeneous refinement, and subsequent non-uniform homogeneous refinement of a final class with C3 symmetry. To better resolve the binding interface, we used symmetry expanded particles for focused refinement of one Fab and the region it bound on the F protomer. Finally, both global and focused maps were sharpened using DeepEMhancer (Sanchez-Garcia et al., 2021). For model building, we used a crystal structure of hMPV F (PDB ID: 5WB0) and a Fab model generated by SAbPred server (Dunbar et al., 2016) to build into the cryoEM maps using UCSF ChimeraX (Pettersen et al., 2021). Both global and focused models were built further and iteratively refined using a combination of Coot (Casañal et al., 2020), Phenix (Adams et al., 2010), and ISOLDE (Croll, 2018). The detailed workflows of cryo-EM data processing and data validation are presented in Figures S6A, S6E, and S6F.

HMPV F – ADI-61128 – ADI-61026 micrographs were imported to cryoSPARC Live v3.2.0 (Punjani et al., 2017) and processed for motion correction, CTF estimation, micrograph curation, particle picking, and particle curation via iterative rounds of 2D classification. The curated particles in corresponding micrographs were further processed in cryoSPARC v3.2 to obtain a final global reconstruction with additional rounds of 2D classification, *ab initio* reconstruction, iterative rounds of heterogeneous refinement, non-uniform refinement, and a subsequent non-uniform homogeneous refinement after uncropping the particles. For modelling we used a single hMPV F protomer bound by ADI-61026 from our trimeric cryo-EM structure and an ADI-61128 Fab model generated by ColabFold (Evans et al., 2022; Mirdita et al., 2022)to dock into the cryo-EM map using UCSF ChimeraX (Pettersen et al., 2021). The detailed workflow of cryo-EM data processing is presented in Figure S5A.

Negative stain electron microscopy

Using the molecular weight of monomeric hMPV F for calculations, the DS-CavEs2 hMPV prefusion F construct was incubated with a 1.2-fold molar excess of purified ADI-61105 Fab for 10 min at room temperature before being moved to ice. Sample was diluted with filtered buffer (2 mM Tris pH 8.0, 200 mM NaCl, and 0.02% NaN_3) to a final hMPV F concentration of 0.015 mg/ml immediately before application of 4 μL to a plasma-cleaned carbon film, 400 mesh copper grid (Electron Microscopy Sciences; catalog no. CF400-Cu). After 1 min, sample was blotted from the grid and uranyl acetate pH 7 was used for negative staining of the protein complex. Sample was imaged at 60,000x magnification corresponding to a pixel size of 3.6 Å/pixel using a 200 kV JEOL 2010F transmission electron microscope equipped with a Gatan OneView camera. Particles were selected using cisTEM and imported into cryoSPARC v3.2 (Grant et al., 2018; Punjani et al., 2017) where 2D class averages were generated and used for *ab initio* 3D reconstruction followed by heterogeneous refinement and then homogeneous refinement. For modelling, a crystal structure of hMPV F (PDB ID: 5WB0) and a Fab model generated by ColabFold (Evans et al., 2022; Mirdita et al., 2022) were docked into the 3D volume using UCSF ChimeraX (Pettersen et al., 2021).

QUANTIFICATION AND STATISTICAL ANALYSIS

All statistical analyses were performed in GraphPad Prism 9. Detailed descriptions of all statistical tests are provided in figure legends. No data was excluded from statistical analysis and significance was defined by a p value of less than or equal to 0.05 for all tests.